FUNCTIONAL MRI OF THE KIDNEYS

INVESTIGATING MINIMALLY INVASIVE STRESSORS FOR FUNCTIONAL MRI OF THE KIDNEYS

By

MARLA A. SHAVER, B.Eng.

A Thesis

Submitted to the School of Graduate Studies

in Partial Fulfilment of the Requirements

for the Degree

Master of Applied Science

McMaster University

MASTER OF APPLIED SCEINCE (2013) McMaster University

(School of Biomedical Engineering) Hamilton, Ontario

TITLE: Investigating Minimally Invasive Stressors for Functional MRI of the Kidneys

AUTHOR: Marla A. Shaver, B.Eng.(McMaster University)

SUPERVISOR: Michael D. Noseworthy, Ph.D.

NUMBER OF PAGES: xv, 83

Abstract

The health of the kidneys is vital for the production of concentrated urine, regulation of ion and acid-base balance and regulating blood pressure. Chronic kidney disease (CKD) has an annual mortality rate of 22% and can cause secondary complications including hypertension, anemia, secondary hyperparathyroidism, and malnutrition. Currently clinical diagnosis and evaluation of CKD involves blood and urine testing and biopsy. MRI is not currently used to image CKD, but there is a large interest in developing MRI techniques to design a minimally invasive test for kidney function and to further understand the disease. Functional MRI (fMRI) has been utilized in studies with varying degrees of success. Usually, renal fMRI refers to single time-point images reflecting tissue oxygenation. Using time series information to measure oscillations in the system may offer additional information and be better able to show changes in the kidneys as a result of disease.

In this thesis, blood oxygen level-dependent (BOLD) MRI and diffusion weighted imaging (DWI) were used to investigate the effects of breath holding and water loading on kidneys. First, BOLD MRI was used to determine whether breath holding has measurable effects on BOLD signal intensity. Next, water loading was considered as a tool for studying how the kidney reacts to stress: in this case, diuresis. DWI was used in an attempt to measure changes in diffusion and perfusion shortly after water loading, and fractal analysis was performed on BOLD time series to look for changes in microcirculation after water loading in kidneys.

Breath holding results showed no effect on temporal BOLD signal intensity in young, healthy subjects. A significant decrease in signal intensity is measured in the kidney of a single subject with impaired renal function. This result suggests that breath holding effects may need to be considered when subjects of different age and/or disease state are compared. Although the renal BOLD signal was found to have fractal characteristics, no changes were measured using this technique between pre- and post-water loading scans during the time period examined. Because the signal appears to behave fractally, this technique may be a good candidate for similar kidney function studies in the future. DWI also remained unchanged as a result of water loading during the post-water loading time period examined.

Acknowledgements

I would like to thank my supervisor, Dr. Michael Noseworthy, for his guidance and for giving me the opportunity to be a part of his lab. I would like to thank everyone in the Imaging Research Centre for sharing their expertise and insight and for keeping me motivated throughout the past two years. A special thank you to the MR technologists at St. Joseph's for helping with the practical considerations of MRI. Finally, I would like to thank my family for getting me to where I am.

Table of Contents

List of Figures

List of Tables

List of Notations and Abbreviations

χ	Magnetic susceptibility
γ	gyromagnetic ratio
τ	Window length
A	Amplitude
ADC	Apparent diffusion coefficient
ADH	Antidiuretic hormone
ANOVA	Analysis of variance
ANP	Atrial natriuretic peptide
ARF	Acute renal failure
B_0	Main magnetic field strength
BOLD	Blood oxygen-level dependant
B_{int}	local magnetic field
CBF	Cerebral blood flow
CKD	Chronic kidney disease
CKD-EPI	Chronic kidney disease epidemiology collaboration
CRF	Chronic renal failure
CT	Computed tomography
D	Coefficient of diffusion
D^*	Pseudo-diffusion coefficient
DCE	Dynamic contrast enhanced
deoxyHg	Deoxygenated hemoglobin
dL	decaliter
DWI	Diffusion weighted imaging

EARD	End stage renal disease
eGFR	Estimated glomerular filtration rate
EPI	Echo planar imaging
f	Fraction of perfusion
f_w	tissue NMR visible water content fraction
FD	Fractal dimension
FFT	Fast Fourier transform
fBm	Fractional Brownian motion
fGn	Fractional Gaussian noise
FIESTA	Fast imaging employing steady state acquisition
fMRI	Functional magnetic resonance imaging
G	Gradient field strength
Gd	Gadolinium
GE	General electric
GFR	Glomerular filtration rate
GRE	Gradient recalled echo
H	Hurst coefficient
IVIM	Intravoxel incoherent motion
JB	Jarque-Bera
kg	Kilogram
$< l >$	mean capillary length
L	Total capillary length *or* liter
MDRD	Modification of diet in renal disease study
mg	Milligrams
mGRE	Multiple gradient-recalled echo

min	Minute
ml	Milliliter
NEX	Number of excitations
mm	Millimeter
ms	Millisecond
MRA	Magnetic resonance angiography
MRI	Magnetic resonance imaging
NMR	Nuclear magnetic resonance
NSF	Nephrogenic systemic fibrosis
P_{AO_2}	Partial pressure of oxygen in the blood
$R2^*$	Effective transverse relaxivity
RAS	Renal artery stenosis
REB	Research ethics board
RF	Radio frequency
ROI	Region of interest
s	Second
S	Signal intensity
S_0	Reference signal intensity
SCR	Serum creatinine
SD	Standard deviation
SNR	Signal to noise ratio
T	Tesla
T_2^*	Transverse relaxation parameter (effective)
T2	Transverse relaxation
TE	Echo time
TR	Repetition time

Chapter 1

Introduction

The health of the kidneys is vital for maintaining homeostasis and removing waste in the body. They are responsible for the production of concentrated urine, regulation of acid-base and ion balance and regulating blood pressure. Chronic kidney disease (CKD) has an annual mortality rate of 22% and can cause secondary complications including hypertension, anemia, secondary hyperparathyroidism, and malnutrition (3). CKD can result from various preexisting conditions: most commonly diabetes and hypertension (3). Once kidney damage occurs, hyperfiltration in the remaining viable nephrons in an attempt to maintain the glomerular filtration rate (GFR) causes the disease to propagate.

Chronic kidney disease is classified as having one of the following markers for three months or longer:

1. GFR of less than 60 mL/min/1.73 m^2, with or without visible kidney damage, or

2. Pathological abnormalities or markers of kidney damage found in

blood or urine tests or with medical imaging (3). Imaging techniques such as ultrasound or computed tomography may show cysts, tumours or size disparities in the kidney.

Typical GFR in healthy individuals is 127 mL/min/1.73 m^2 in men and 118 mL/min/1.73 m^2 in women, and decreases with age (3). This value can very and must be below 60 mL/min/1.73 m^2 to indicate CKD without any other abnormalities. CKD is divided in three stages based on GFR, which presents a problem, as GFR is difficult to measure. The gold standard method is inulin clearance, but this requires intravenous infusion and timed urine collection, which is not practical clinically. Creatinine clearance is another method of estimating GFR. Creatinine is filtered in the glomerulus and is also excreted in the proximal tubule, and so tends to over estimate GFR by approximately 20%.

Magnetic resonance imaging (MRI) is not performed clinically to evaluate CKD. Typical motivations for renal MRI are renal masses and blockages. A number of studies have attempted to measured GFR using dynamic contrast enhanced (DCE) MRI with varying success (4; 5; 6; 7). A review of these methods found that reproducibility and accuracy were poor overall (8). A major concern with these methods, regardless of their success, is that gadolinium (Gd) contrast agents were used. Patients with impaired kidney function

(typically patients with GFR <30 mL/min/1.73 m^2) are at risk of developing nephrogenic systemic fibrosis (NSF) when exposed to gadolinium-based contrast. NSF presents as fibrotic lesions in the skin causing pain and muscle weakness. Eventually, this fibrosis affects skin, joints, skeletal muscles, testes, kidney, myocardium, and dura (9). Because of this risk, impaired GFR is a contraindication for Gd-based contrast administration.

In this thesis, functional MRI is proposed as a method to evaluate kidney function. Not necessarily to measure GFR, but as a means to further understand renal physiology and as a potential novel method for non-invasively evaluating kidney function. Blood oxygen level dependent (BOLD) MRI and diffusion weighted imaging (DWI) are used to study the effects of breath holding and water diuresis on the renal MR signal. These stressors are used to cause a change in the MR signal without the introduction of any drugs. To evaluate these stressors, temporal BOLD signal intensity changes (Chapter 2), bi-exponential diffusion modelling (Chapter 3), and fractal analysis (Chapter 4) are used. We expect that healthy kidneys may respond differently to these stresses than kidneys with impaired function because of a reduced ability to react to environmental changes in kidneys where CKD exists.

1.1 The Kidney: Normal Function and Pathology

1.1.1 Normal Anatomy

The kidneys can be divided into three main sections: the renal cortex, the renal medulla and the renal pelvis, shown in figure 1.1. The cortex is the outermost layer, followed by the medulla, made up of eight to eighteen renal pyramids pointing inward towards the renal pelvis. Within the cortex and medulla are approximately one million nephrons: the functional unit of the kidney. Urine that is produced in the nephrons is drained into the renal pelvis, from which it exits the kidneys through the ureter.

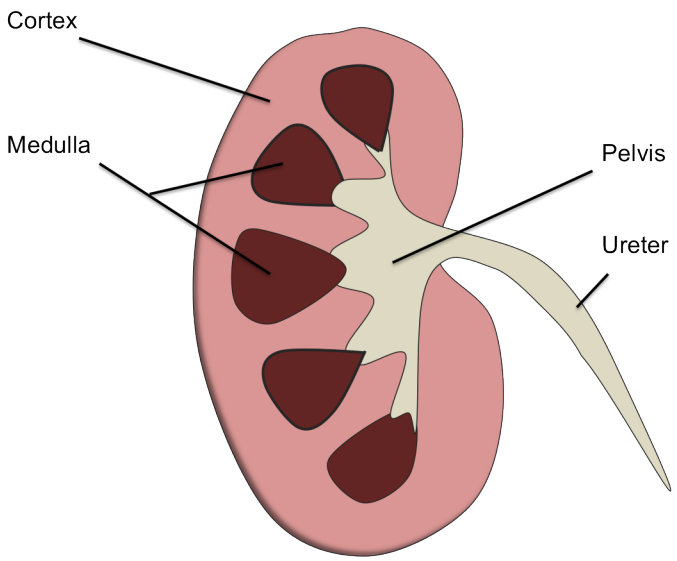

Figure 1.1: Coronal cross section of the right kidney showing gross structures.

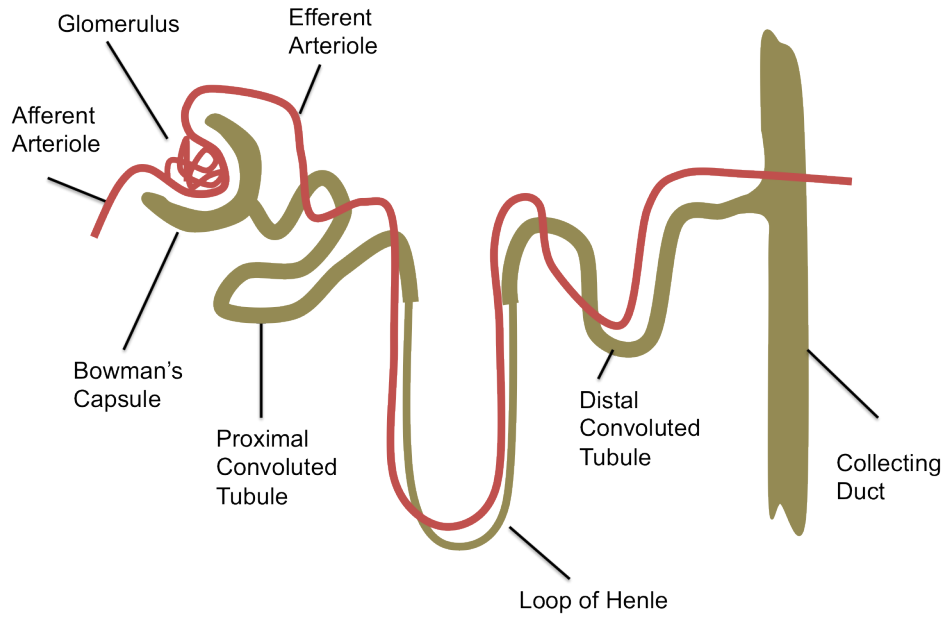

Figure 1.2: A single nephron with associated vasculature.

Each kidney is normally supplied by a single renal artery, which branches into seven arteries to supply the entire kidney. These arteries branch to make one afferent arteriole for each nephron (figure 1.2). The capillary networks made by the branching of afferent arterioles are called glomeruli: the site of filtrate formation. After the blood has passed through the glomerulus, the capillaries join back together to make efferent arterioles, which lead to peritubular capillaries that extend alongside the nephrons. The blood supply to the kidney as well as the ureter, lymphatic vessels and nerves enter and exit the kidney through the renal hilum, on the concave side of the kidney.

Once the filtrate is separated in the glomeruli, it goes through the nephrons to be concentrated into urine. The nephron is made up of the Bowmans capsule, proximal convoluted tubule, the loop of Henle (made up of the thin descending and thick ascending limbs), and distal convoluted tubule (figure 1.2). Most nephrons originating in the superficial or mid cortex extend just to the outer medulla, or turn before reaching the medulla at all. Nephrons originating near the corticomedullary boundary are longer and extend to the inner medulla.

The collecting duct extends from the distal convoluted tubule of the nephron in the outer cortex, through the medulla to the ureter. It is divided into three segments: the cortical, outer medullary and inner medullary collecting duct. These segments differ in their cellular makeup and function.

1.1.2 Renal Metabolism

The kidneys are the second most oxygen-demanding organ per gram of tissue in the body (10). This oxygen demand is a result of active transport to concentrate urine. The sodium pump (Na+ -K+ ATPase) is used for epithelial transport of sodium out of a cell and potassium into the cell. It requires 1 ATP to transport 3Na+ and 2 K+. Other energy-consuming transport molecules found in the nephron epithelium are H+-K+-ATPase, Ca2+-ATPases, and

H+-ATPases (11), which are important for maintaining homeostasis and do not play as important of a role in urine concentration. The thick ascending tubules have a particularly large rate of sodium transport and therefore use large amount of oxygen (12).

Regulating tissue oxygenation is a concern in the kidney, particularly in the medulla, which functions in a hypoxic environment. Unlike other organs, the blood supply to the kidneys is regulated to control blood volume and composition and not to meet oxygen demands of the tissue. Instead, to stabilize tissue oxygenation, the kidney must alter oxygen consumption and distribution of oxygen delivery. Tubuloglomerular feedback to control tubular flow rate and tissue oxygenation is slow, and so the system tends to oscillate with a period of about 30 seconds (11).

1.1.3 Mechanism of Urine Formation

The first step in urine formation is filtration of the blood in the glomerulus. All parts of the blood except the formed elements (red and white blood cells) and most proteins are filtered into the glomerular capsule to make up the filtrate. Most of this filtrate will eventually be reabsorbed back into the blood. Re-absorption begins in the proximal convoluted tubule. Here, glucose, amino acids, metabolites and electrolytes are reabsorbed. The active transport of

sodium ions into the blood stream causes passive re-absorption of water along the osmotic gradient. In the loop of Henle the remaining filtrate is concentrated by exchange of electrolytes and re-absorption of water; again, sodium is reabsorbed by active transport. Sodium is also reabsorbed in the distal convoluted tubule if aldosterone is present. Secretion of waste products such as ammonia and hydrogen ions from the peritubular capillaries takes place in the nephron as well.

The re-absorption of sodium and water are controlled by two separate mechanisms. Blood pressure is regulated by the renin-angiotensin aldosterone system. When blood pressure is too low, renin is released from juxtaglomerular cells. Renin converts angiotensinogen in blood to angiotensin I, which is then converted to angiotensin II in the lungs. Angiotensin II stimulates the production of aldosterone in the adrenal cortex, which acts on juxtaglomerular cells to increase the re-absorption of water and sodium and decreases the release of renin. Another role of angiotensin II is to cause blood vessels to constrict, further increasing blood pressure, and to stimulate the release of antidiuretic hormone (ADH). ADH acts on the distal tubule and collecting ducts to increase re-absorption of water by making these vessels more permeable. To reduce blood pressure, re-absorption of sodium from the nephrons to the capillaries must be restricted. This is achieved by atrial natriuretic peptide

(ANP). ANP also acts to inhibit renin secretion and decrease sodium reabsorption. With more sodium in the filtrate, water will leave the capillaries by osmosis.

1.1.4 Induced Diuresis

Inducing diuresis has been used as a method of stressing the kidney while studying kidney physiology. Common ways to induce kidney diuresis are with drugs, such as furosemide or acetazolamide (13), or with large quantities of water. Furosemide works in the ascending limb of the loop of Henle to inhibit transport and therefore impair the reabsorption of water (14). These effects can be seen as a decrease in oxygen consumption in the renal medulla causing a decrease in T2* in BOLD MR (13; 15). Acetazolamide is also a diuretic, but it works in the proximal tubule. Again, it has been shown to decrease T2* by reducing oxygen consumption, but this effect is seen only in the cortex and only a small change is produced (13).

Consumption of large amounts of water without any salt lowers plasma sodium concentration and results in increased intracellular and extra cellular fluid volumes (16). The body's response to this is to suppress the release of anti diuretic hormone (16). ADH suppression decreases re-absorption of water. If water and salt are consumed at a concentration isotonic to that in

the blood stream, the juxtaglomerular cells will produce less renin (16). This along with the increase in atrial natriuretic peptide causes blood vessels to dilate in an effort to decrease blood pressure back to normal (16). An increase in sodium excretion in the nephrons will draw water into the filtrate to balance fluid volumes (16). The timing of water loading effects has been shown to be subject dependent (17; 18).

Water loading has been shown to increase medullary P_{AO_2} in young people (13). This effect is not seen in older people (19) or people with diabetes mellitus (20). The time required for the effects of water loading to be measurable with BOLD MRI varies between individuals, but in most people, effects are seen after approximately one hour (17). Few effects of water loading have been measured with DWI. It has, however, been demonstrated that the kidneys have higher ADC when subjects are hydrated as compared to the same subjects in a dehydrated state (21; 18).

1.1.5 Pathology - Chronic Kidney Disease

The stages of chronic kidney disease (CKD) are characterized by estimated glomerular filtration rate (GFR), with stage 1 kidney disease patients having a GFR of greater than 90 mL/min but with visible signs of kidney damage in medical imaging (for example cystic lesions or stenosis), blood or

urine tests. From there, the stage increases with decreasing GFR. Stage 5 is end stage renal disease (ESRD) wherein patients having a GFR of less than 15 mL/min (22). The main causes for CKD are diabetic nephropathy, chronic glomerular disease, polycystic kidney diseases and hypertension (16). GFR is estimated based on serum creatinine (SCR) levels. One of the most widely used equations for estimating GFR is the Modification of Diet in Renal Disease (MDRD) equation (23), based on the Cockcroft-Gault equation (24):

$$\begin{aligned}\text{GFR (mL per min. per } 1.73m^2) = 170 \times [P_{Cr}]^{-0.999} \times (age)^{-0.176} \\ \times 0.822 \text{ if female} \times 1.180 \text{ if African-American} \times [SUN]^{-0.170} \times [Alb]^{0.318}\end{aligned} \tag{1.1}$$

Here, P_{Cr} is serum creatinine concentration (mg/dL), SUN is serum urea nitrogen concentration (mg/dL) and Alb is serum albumin concentration (g/dL). All of the values in this equation can be measured from a blood test. The Chronic Kidney Disease Epidemiology Collaboration (CKD-EPI) equation (25) is another method of calculating GFR that is gradually gaining popularity (Eq. 1.2).

$$\text{GFR (mL per min. per } 1.73m^2) = 141 \times min(Scr/\kappa, 1)^{\alpha} \times max(Scr/\kappa, 1)^{-1.209} \times 0.993^{age} \times 1.018 \text{ if female} \times 1.159 \text{ if African-American} \tag{1.2}$$

In this equation, Scr is serum creatinine, κ is 0.7 for females and 0.9 for males, α is -0.329 for females and -0.411 for males, and min and max refer to either the minimum or maximum of Scr and 1 respectively. The CKD-EPI equation has been shown to be as accurate as the MDRD equation for GFR less than 60 mL/min/$173m^s$ and more accurate for higher GFR (25).

The symptoms of CKD are not usually present and recognized until the disease has progressed quite far and there is already significant damage to the kidneys, therefore the disease is often found during a routine health examination or in preparation for treatment of other medical conditions. Some of the symptoms of CKD are tiredness, anorexia, nausea and vomiting, itching, nocturia, oliguria, haematuria, frothy urine, and loin pain (26). The most common tests for CKD are plasma creatinine and urine dipstick tests.

Urine testing looks for elevated albumin excretion, microscopic haematuria, and proteinuria. All of these things indicate CKD when elevated. With-

out a urine or blood test it is impossible to quantify the progression of CKD. The plasma creatinine test is used to estimate GFR. Creatinine cleared by the kidneys is a relatively good indicator for the filtering rate of the kidneys because it is almost completely excreted in the urine. This test is not very sensitive when decrease in GFR is very low, and it is only completely accurate if the kidney is healthy (27). For both of these reasons, estimation of GFR is not an ideal measure of kidney function, but it is still considered the standard. Another disadvantage of using estimated GFR (eGFR) to test kidney function is that it measures the total function of all nephrons in both kidneys and is therefore not useful in identifying the proportion of damaged kidney and whether both or only one kidney is malfunctioning. Other modalities for evaluating kidney function include ultrasound for renal failure, proteinuria/nephrotic syndrome, and renal infection, computed tomography (CT) for renal stones, renal infection, and retroperitoneal fibrosis and magnetic resonance angiography (MRA) for renal artery stenosis.

1.2 BOLD MRI of the Kidney

Blood oxygen level-dependent (BOLD) MRI utilizes paramagnetic deoxygenated hemoglobin (deoxyHg) as an intrinsic contrast agent. The susceptibility difference between deoxyHg and the surrounding tissue causes inhomogeneities in the local magnetic field:

$$B_{int} = B_0(1 - \chi), \tag{1.3}$$

where B_0 is the main magnetic field strength and χ is susceptibility. This introduced inhomogeneity results in a dephasing of protons close to the blood and thus an attenuation in the T2* weighted signal.

$$\frac{1}{T2*} = \frac{1}{T2} + \gamma \Delta B_0, \tag{1.4}$$

Here, γ is the gyromagnetic ratio. The increase in T2* is seen in the image as an attenuation that reflects the ratio of oxygenated to deoxygenated hemoglobin, which can be affected by blood flow, blood volume, hematocrit and oxygen metabolism.

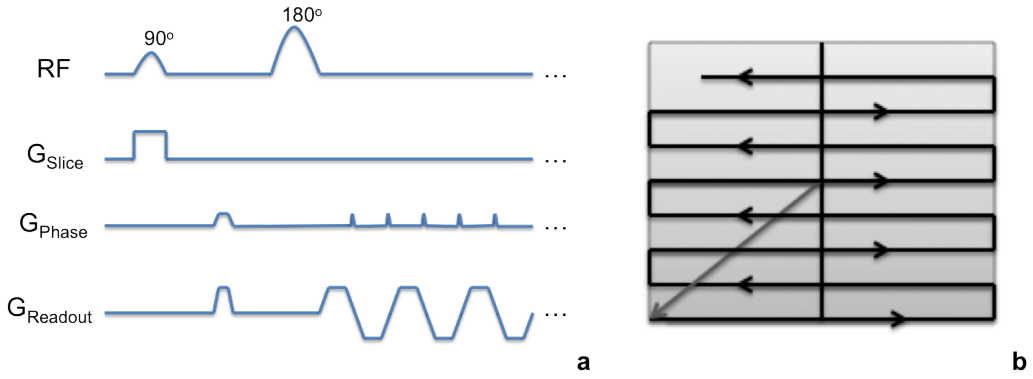

Figure 1.3: (a) A spin echo EPI pulse sequence. The readout gradient flips back and forth to create a pulse train, filling all of k space in a single excitation and (b) the resultant k-space trajectory.

BOLD acquisition uses T2*-weighted echo planar imaging (EPI), a fast, single-shot acquisition method. An example EPI pulse sequence is shown in figure 1.3 (a). A radio frequency (RF) excitation is applied at the same time as the slice select gradient. The readout gradient is then switched between positive and negative to create an echo train, allowing all of k space to be filled (i.e. acquiring an entire image slice) in a single RF excitation. Figure 1.3 (b) shows the k space trajectory that results from this pulse sequence shown. Alternatively, k-space can be sampled using a spiral acquisition, which has the advantage of being less sensitive to patient motion. Also, multiple excitations can be used to sample k space to increase resolution or field of view. Disadvantages of EPI sequences include sensitivity to susceptibility differences causing distortion and reduced signal to noise (SNR).

Kidneys are susceptible to ischemic injury, particularly the renal medulla, which makes BOLD MR a potentially useful tool for evaluating kidney function (28). BOLD imaging of the kidney has been studied since 1996, when Prasad *et.al* published their first paper showing its utility in imaging renal oxygenation (13). They examined the change in R2* (R2*=1/T2*) after administration of one of three diuretics: furosimide, acetazolamide or water. Their experiment showed that furosemide, a loop diuretic, caused a decrease in medullary R2*, acetazolamide, another diuretic that interferes with bicarbonate reabsorption in the kidneys, caused no significant change in any part of the kidney and water diuresis caused a significant decrease in medullary R2* in five out of six patients. R2* mapping is a common technique used in BOLD kidney studies. This is a single time point image that requires measurements at various echo times, ideally acquired in a single breath hold. For this technique, multiple gradient-recalled echo (mGRE) sequences can be used (29). R2* values are linearly correlated with tissue P_{AO_2} (30), which can be affected by changes in nephron oxygen consumption or perfusion changes. A reproducibility study of healthy kidneys by Simon-Zoula *et.al* found a small but significant difference in measured R2* between left and right kidneys, with most subjects showing higher values in the left kidney (31). They also observed a positive correlation between R2* and age.

In the kidney, one interpretation of the intensity of the R2* signal is that when the kidney is reabsorbing more sodium by active transport, more oxygen will be used resulting in a higher concentration of deoxyHg, and the signal will be larger (32). If the kidney's ability to reabsorb sodium is some how compromised, the expected signal change is not observed. The change in R2* after administration of various drugs has also been used to study disease (19; 33). In the case of hypertension, it has been shown that hypertensive rats show no R2* response to nitric oxide synthesis inhibitor, while healthy rats show a change in R2* (34). Similarly, where water diuresis will cause a decrease in R2* in young healthy patients, less change is observed in diabetic or elderly patients (19; 33). This response in diabetic patients is thought to be a result of hyperfiltration (34). Another conclusion that has been made is that an increase in R2* can be correlated with arterial stenosis (34). In this situation, the reduction in blood flow results in more time for oxygen to be taken from the blood as at passes through the kidney.

R2* mapping has been investigated as a means of imaging chronic kidney disease (CKD). A 400 patient study by Michaely *et.al* found no correlation between R2* value and kidney disease stage (35). These results contradict the results of other studies and the hypothesis that chronic hypoxia is common to all end stage CKD (36). A significant positive correlation has been shown

between eGFR and T2* in patents with non-diabetic CKD (37). In the same study, this correlation was not present in patients with diabetic nephropathy, although T2* values taken from those subjects were often lower than in healthy volunteers. In another study, a significant correlation was found between eGFR and R2* in patients with diabetic nephropathy (38). They saw a positive correlation between medullary R2* and eGFR and a negative correlation between cortical R2* and eGFR. This correlation may have been missed in the previously discussed study because measurements from the cortex and medulla were analyzed together. The discrepancy between Michaely *et.al* and other studies may exist because this study did not separate groups of CKD patients based on the cause of kidney disease. As pointed out by Neugarten (39), renal oxygenation may not reflect the stage of the disease directly, but may also depend on the underlying etiology of the disease. BOLD signal can be influenced by oxygen supply, oxygen consumption, blood flow, blood volume, hematocrit and P_{AO_2}. R2* is influenced by vessel geometry and pulse sequence parameters (34). As a result, R2* maps can be interpreted in many ways, and assumptions need to be made based on the situation in order to make a practical conclusion.

1.3 Renal Diffusion Weighted Imaging

Diffusion weighted imaging (DWI) uses strong magnetic field gradients to sensitize the images to molecular diffusion of water. The underlying principle is that molecules that are moving will experience different amounts of dephasing and rephrasing when the diffusion gradients are applied, and will cause an attenuation of signal intensity. The function of the nephrons is largely a function of water transport, and therefore, DWI is likely to provide useful information on the function of the kidneys.

An example of the timing of diffusion gradients in an echo planar imaging (EPI) pulse sequence is shown in figure 1.4. Identical diffusion gradients (shown shaded) are placed on either side of the 180^o pulse in a normal spin echo EPI sequence. By changing the strength in each of the three orthogonal slice, readout and phase directions, the sequence can be sensitized to diffusion in any direction. If a gradient echo EPI sequence is used, the second lobe of the diffusion-weighting gradient will be the same shape as the first but with negative amplitude. The diffusion weighting depends on the strength and duration of the gradient and the separation of the diffusion gradient lobes. Increasing the gradient amplitude as opposed to duration has the benefit of reducing TE, which reduces signal loss from T2 relaxation. Using the maximum slew rate

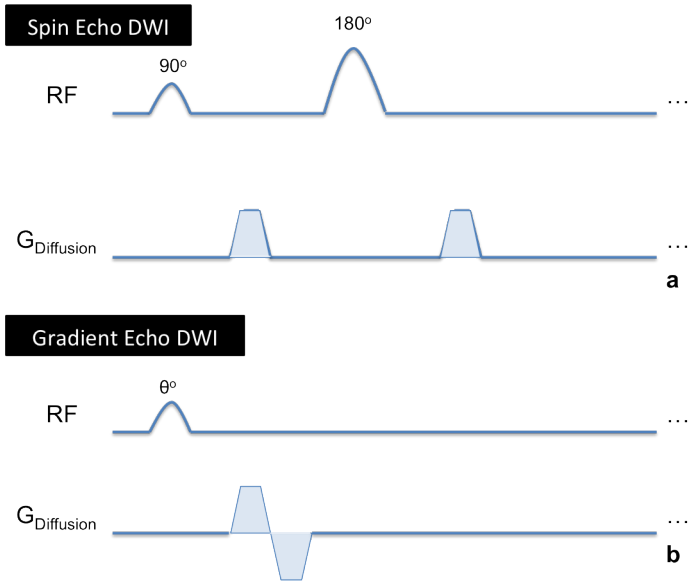

Figure 1.4: Pulse sequence timing diagram showing diffusion weighting gradients (shaded) applied (a) on either side of the 180^o pulse of the spin echo EPI sequence and (b) after the RF excitation of a gradient echo EPI sequence (b). Diffusion gradients can be applied at varying strengths in the slice, readout and phase directions to sensitize to diffusion in any direction.

can also decrease TE, but there are limits on slew rate to prevent peripheral nerve stimulation and eddy currents.

The signal arising from DWI sequences is commonly modelled by

$$S = S_0 e^{-bD}. \tag{1.5}$$

In this equation, S_0 is the signal with no diffusion weighting, S is the signal with diffusion weighting, b is the b-value that determines the amount

of diffusion weighting (in s/mm^2) and D is the diffusion coefficient in the direction of the diffusion gradient (in mm^2/s). The diffusion that is measured in DWI is influenced by both diffusion and perfusion in the tissue, and for this reason is typically referred to as the apparent diffusion coefficient (ADC). In the kidney, there is a strong contribution to the DWI signal decay from perfusion. For this reason, a bi-exponential decay model can more accurately represent the data (40) and using this model can reduce the variability in ADC values in healthy kidneys (41). The bi-exponential decay can be modelled by equation 1.6 (42):

$$S = S_0((1-f)e^{-bD} + fe^{-b(D+D*)}) \tag{1.6}$$

where f is the fraction of pseudodiffusion (or perfusion fraction), D is the coefficient of pure diffusion, and D* is the coefficient of the pseudodiffusion portion. In some studies, D_P is calculated instead of D*. D_P is equal to D+D*. Measurements are made at many different b-values and the resultant data are fit to the bi-exponential model. The introduction of the perfusion fraction and pseudodiffusion coefficient allows for insight to be gained on tissue microcirculation, or perfusion. This technique is known as intravoxel incoherent motion

(IVIM). An example set of typical values reported in literature are f: 0.234 ± 0.0934 , D: 0.0021 ± 0.0003 mm^2/s and D*: 0.1108 ± 0.0124 mm^2/s (1).

b-value selection can be important for result accuracy. A recent work by Zhang *et.al* (43) has suggested that once the bi-exponential model has been verified for a particular tissue using a large number of distributed b-values, focused at low values, their set of optimal b-values can provide increased accuracy in measurements. They reported that for healthy renal tissue, optimal b-values are 0, 52, 268 and 750 s/mm^2 and for renal lesions 0, 51, 259 and 800 s/mm^2, with any additional b-values obtained being repetitions of the higher b-values. They also reported that as the number of b-values increase, the distribution of those b-values becomes less important.

Work done by Le Bihan and Turner in 1992 attempted to find the relationship between IVIM characteristics and classical perfusion measurements using tracers in the brain (44). They suggested that since f is related to blood volume and D* is related to blood velocity, than these parameters can be combined to describe tissue microcirculation. Specifically,

$$CBF = (\frac{6f_w}{L < l >})fD*, \tag{1.7}$$

where f_w is tissue NMR visible water content fraction, L is total capillary length, and $< l >$ is mean capillary segment length. Given that the value in parenthesis is constant for a specific tissue, the product $fD*$ can be used to evaluate changes in perfusion.

Previous work in renal DWI has shown that the mean ADC in tumors is significantly lower than that in healthy tissue (45). A correlation between GFR and ADC in hydronephrotic kidneys has been demonstrated (46). The same correlation was not strong in healthy kidneys. Namimoto *et.al* studied ADC in chronic renal failure (CRF), acute renal failure (ARF) and renal artery stenosis (RAS) (47). They found that all three diseases affect ADC. The ADC values in the cortex and medulla of CRF kidneys were significantly lower than in healthy kidneys. In ARF kidneys, the ADC was significantly lower than that of healthy kidneys in both the cortex and medulla, and in the cortex, it was significantly higher than that of kidneys with CRF.

As with many abdominal imaging techniques, respiratory motion is a challenge that must be considered. Some strategies that have been implemented include respiratory triggering, breath holding and using free breathing acquisition with subsequent motion correction. Measured diffusion coefficients can also be impacted by blood flow. There are statistically significant differences in measured ADC values when measurements are taken during maximum

or minimum blood flow (48). Cardiac triggering can be used during DWI acquisition to control for these differences, but this will increase the time of the scan. Increasing scan time is particularly problematic when breath holding is used to reduce abdominal motion, and when cardiac triggering is pared with respiratory triggering, the scan time can become quite long. Another factor affecting diffusion measurements in the kidney is hydration. ADC values have been found to be lower in dehydrated kidneys (21; 18).

Chapter 2

Effects of Breath Holding on the BOLD MR Signal

Breath holding is often used as a means of reducing respiratory motion in abdominal MRI, but little has been done to determine whether this has an affect on the measured signal. In the brain, breath holding effects in the T2*-weighted signal have been studied (49; 50; 51; 52). In a 1.5T MRI, BOLD signal changes of 1-4% were seen in the cortex during a periodic breath holding challenge consisting of repeated segments of 30 second breath holds and 30 seconds of normal breathing (53). During a prolonged breath hold, signal intensity in the cortex began to increase immediately and plateaued after about 30 seconds (53). We imaged young, healthy subjects to see if any such changes could be observed in the kidney.

2.1 Hypothesis

Oxygen delivery to the kidney is a tightly controlled mechanism. Careful control of blood-oxygen level is required to prevent hypoxic injury and to maintain ion gradients necessary for concentration of urine. The kidneys are unique in that oxygen perfusion depends on blood volume and osmolality in the blood and not on the oxygen demands of the tissue. For this reason, we think that it may be possible to measure a decrease in BOLD signal intensity as the oxygen concentration in the perfusing blood decreases as a result of breath holding.

2.2 Methods

2.2.1 Subject selection

Six healthy, young subjects (3 male, 3 female), ages 21-29, and one patient with symptoms of impaired renal function (female, age 62) were scanned for this study. Healthy subjects had no history of kidney disease and were not taking any medication. Signs of renal impairment in the kidney patient were evident from a urine test. Abnormally high protein of 1.0 g/L and albumin/creatinine ratio of 440 mg/L were measured (normal ranges are <0.3 g/L

and <31 mg/L respectively). eGFR of 199 is in the normal range. The patient also had hypertension and was taking a diuretic medication and angiotensin II receptor antagonist as treatment.

2.2.2 Imaging protocol

All images were acquired using a GE Healthcare 3T HD Signa MRI and 8-channel torso phased array coil. Healthy subjects (n=6) were imaged using a T2* weighted BOLD GRE EPI sequence (TR/TE=250/35ms, flip=70^o, FOV=30cm 128x128 matrix, 3 slices 5mm thick, 0mm skip, oblique-coronal plane, 2400 temporal points, 10 minutes total time). The acquisition plane was prescribed from a sagittal multiphase FIESTA. To prevent through plane motion, the coronal oblique imaging plane was selected along the longitudinal axis of the right kidney, the direction of motion during breathing (figure 2.1). Respiratory data was collected simultaneously with BOLD image acquisition using the MRI scanner respiratory bellows. For each subject, two BOLD scans were performed. The first BOLD scan was performed during normal breathing. During the second scan, subjects were instructed to hold their breath for as long as possible, breath when necessary, and repeat for the duration of the 10 minute scan.

Figure 2.1: Plane selection used in data acquisition. Imaging plane is chosen along the long axis of the kidney: the direction of motion during breathing.

The kidney patent was scanned on a General Electric (GE) Healthcare 3T Discovery MR750 MRI (GE Healthcare, Milwaukee, WI) and receive-only 32 channel torso phased array coil. All other scanning parameters were the same and the timing protocol varied slightly. A 10 minute scan during normal breath was acquired: the same as with healthy subjects. To obtain data during breath holding, five separate scans were performed, each 20 seconds in duration (80 time points).

2.2.3 Data analysis

After data collection, the images were processed with a template matching algorithm previously used for kidney analysis (54). This software tracks

a rectangular area selected by the user (Figure 2.2) and outputs a dataset of that area from each time point (Figure 2.3). Regions of interest (ROI) were selected for the renal medulla and renal cortex using AFNI (55), and this data was exported to MATAB (The Mathworks, Natick MA). Using the data collected from the respiratory bellows, duration of the shortest breath hold and start times of each breath hold for each of the healthy subjects were determined. With this information, BOLD data was segmented into individual breath holds. Mean, median, skewness and kurtosis were calculated for each ROI, over time, during each breath hold and using the free breathing scans. Signal intensity time courses for individual breath holds in each ROI were also looked at for temporal trends.

2.3 Results

Breath hold segments were truncated to the length of the shortest breath hold for each healthy subject for statistical analysis. Data from each subject is shown in table 2.1. Mean breath hold duration used was 46.67 seconds (ranging from 22-64s). Subjects completed 6-16 breath holds during the 10-minute scan. Mean BOLD time series from the cortex and medulla of each subject are shown in figure 2.4 and 2.5 respectively. There were no consistent

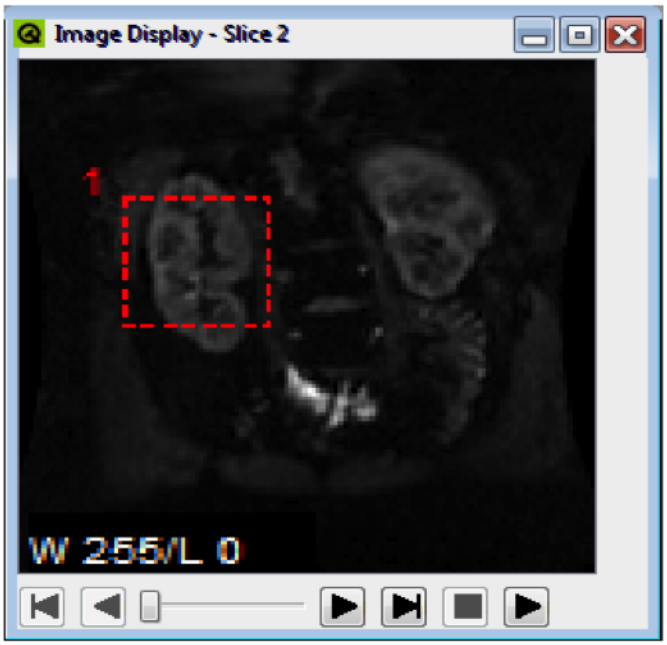

Figure 2.2: Example of a template selection in template matching algorithm used to correct for respiratory motion.

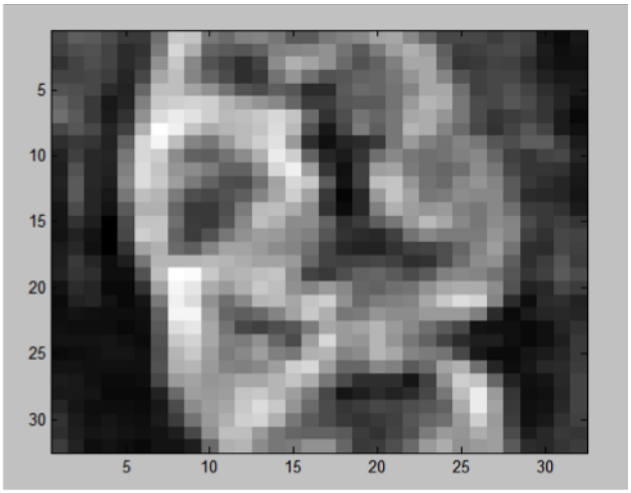

Figure 2.3: Example of resultant field of view after processing with template matching algorithm.

Subject	Shortest Breath Hold (s)	Number of Breath Holds	Free Breathing		Breath Holding	
			Mean ± SD (cortex)	Mean ± SD (medulla)	Mean ± SD (cortex)	Mean ± SD (medulla)
1	64	6	1046.90±18.29	677.89±18.42	818.10±26.72	677.99±16.91
2	36	12	850.98±37.62	518.08±18.71	874.50±33.07	631.26±41.01
3	63	7	576.43±10.01	372.90±10.52	646.82±12.76	410.62±6.89
4	38	10	765.04±38.35	473.52±19.26	572.29±16.43	425.34±25.97
5	57	8	1081.90±77.35	543.53±56.82	544.83±24.06	491.22±8.21
6	22	16	1182.90±23.07	635.23±18.29	1104.10±11.61	627.26±7.24

Table 2.1: Summary of BOLD signal intensities during free breathing and breath holding in healthy subjects.

trends among subjects for either cortex or medulla. The mean signal over all healthy subjects is shown in figure 2.6. No change over time was observed.

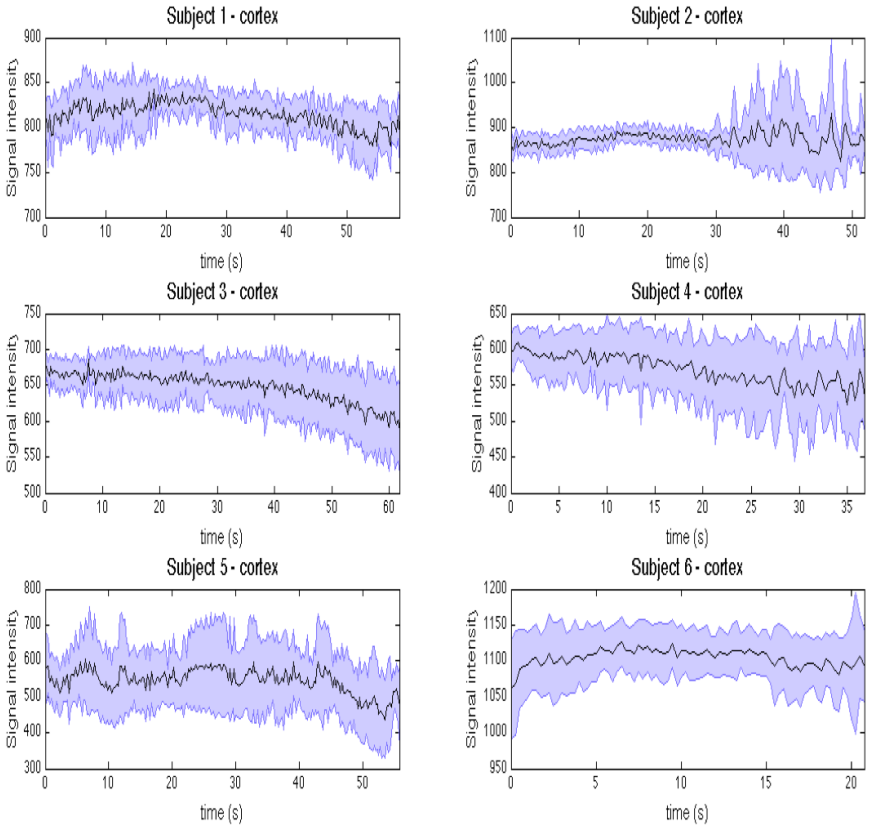

Figure 2.4: Each plot shows mean signal intensity over all breath holds from the cortex of a single healthy subject. The time range is limited to that of the shortest breath hold for that subject. Shaded area represents standard deviation from the mean. Plots from all six healthy subjects are shown.

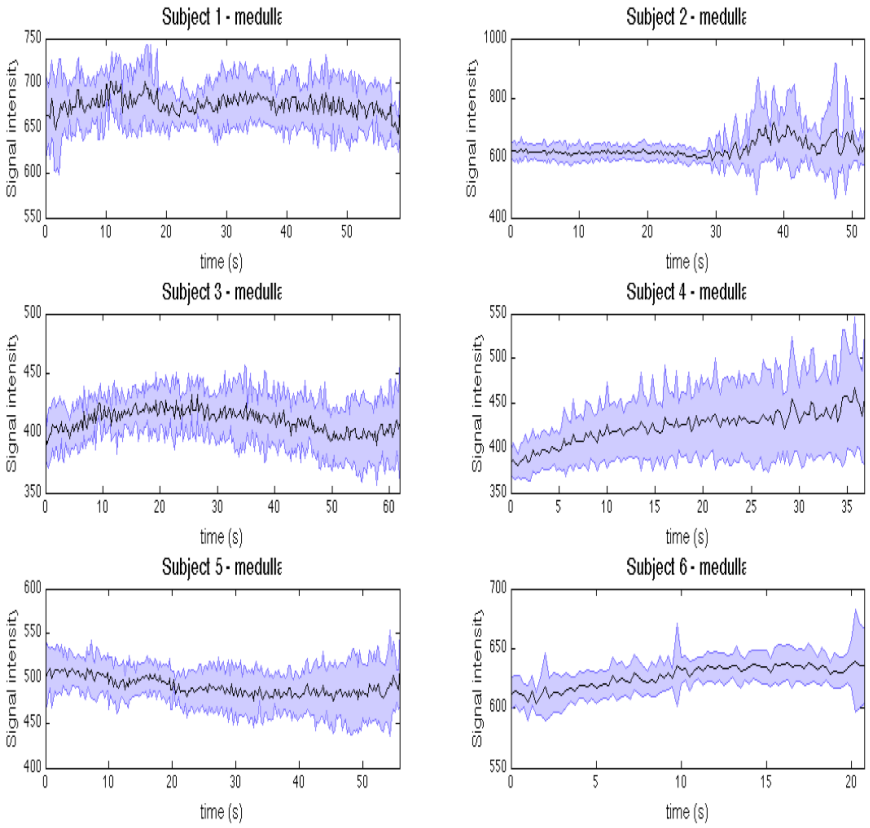

Figure 2.5: Each plot shows mean signal intensity over all breath holds from the medulla of a single healthy subject. The time range is limited to that of the shortest breath hold for that subject. Shaded area represents standard deviation from the mean. Plots from all six healthy subjects are shown.

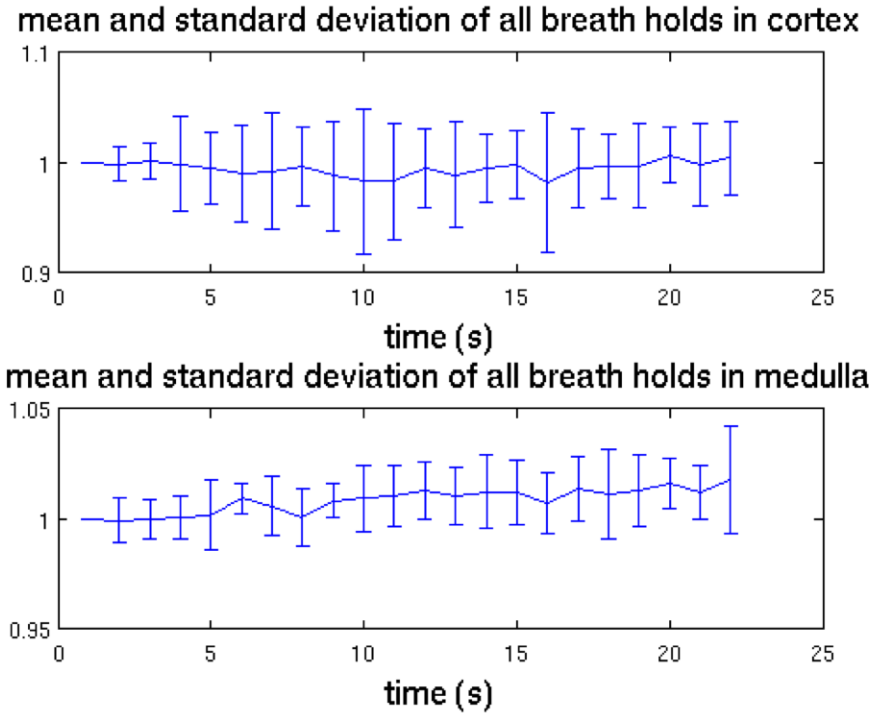

Figure 2.6: Time series data from all breath holds over all healthy subjects averaged together. All data was truncated to duration of the shortest breath hold of all subjects (22s).

The average time course with standard deviation during four of the five breath holds from the CKD patient is shown in figure 2.7. One breath hold scan was discarded due to overt patient motion. A clear negative trend can be observed within in the initial 5 seconds of the breath hold in the renal cortex and medulla.

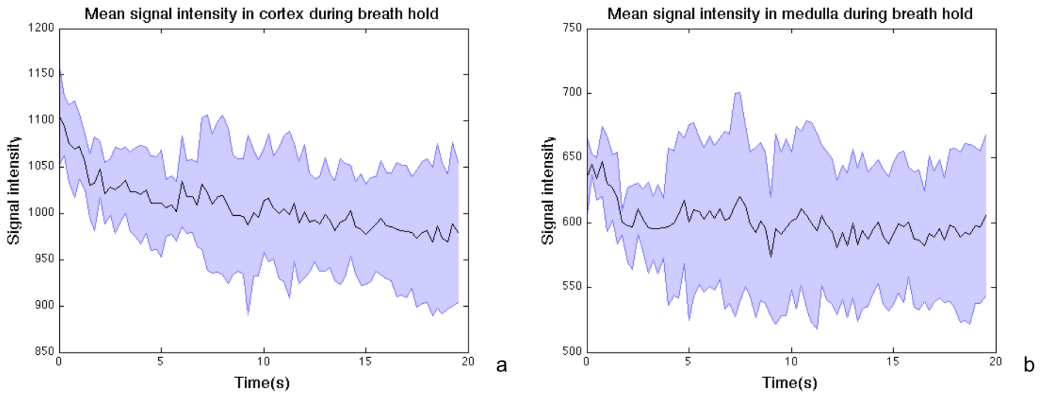

Figure 2.7: Mean signal intensity over all breath holds from the (a) cortex and (b) medulla of a single subject. Shaded area represents standard deviation from the mean.

Mean signal intensity in the cortex and medulla of healthy subjects during breath holding were 760.11 ± 8.54 and 543.95 ± 13.63 respectively. During free breathing scans, mean signal intensity in the medulla and cortex of these subjects were 917.36 ± 23.89 and 536.86 ± 16.57 respectively. A Jarque-Bera (JB) test (testing the null hypothesis of normality) was performed on the set of mean signal intensities from the cortex and medulla of the free breathing and breath holding data. The JB-test did not reject the null hypothesis, so a

parametric paired t-test was performed on the data. A paired t-test showed no significant difference between breath holding and free breathing signal intensities in the cortex (p=0.1399) or medulla (p=0.7898). When the ratio of mean signal intensities of the cortex and medulla was examined, significance increased to p=0.0637. Mean signal intensity in the cortex over mean signal intensity in the medulla was 1.40 ± 0.24 and 1.70 ± 0.18 during breath holding and free breathing respectively.

In the patient with renal impairment, the median signal intensity over all time points was 1002.5 in the cortex and 597.96 in the medulla. The average signal intensity during breath holding after the signal stabilized at 5 seconds was 995.27 in the cortex and 596.78 in the medulla. During the free breathing scan, median signal intensity over all time points was 1331.5 in the cortex and 880.44 in the medulla (Figure 2.8. A wilcoxon test found the difference between signal intensity during free breathing and breath holding to be significantly different ($p < 0.0001$) in both the cortex and medulla.

2.4 Discussion

No difference in signal intensity in the cortex or medulla was observed in BOLD scans acquired while breathing normally or during repeated breath holds in healthy subjects. Measuring the ratio of signal intensity in the cor-

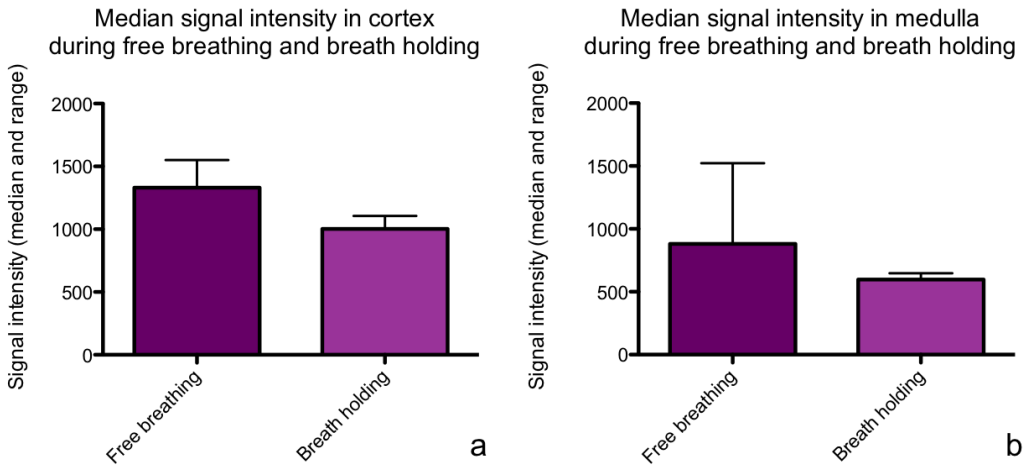

Figure 2.8: Median signal intensity over all time points in (a) the renal cortex and (b) medulla during free breathing and breath holding in a patient with CKD.

tex and medulla increases significance measured by a paired t-test comparing breath holding and free breathing. Looking at breath holding data from individual subjects also did not reveal any trends. A consistent negative trend was, however, observed in the patient with impaired renal function. Looking at the median signal intensity over all time points revealed a 24 and 36 % decrease in signal intensity in the renal cortex and medulla respectively as a result of breath holding. Repeating this experiment with more subjects will help to determine if this trend is consistent in all subjects with impaired renal function and to identify the cause of this trend. A number of factors including age, blood pressure, and medication may be contributing to this difference.

Whether or not this change is occurring because of renal or systemic activity has not been examined.

The possibility of breath holding having measurably different effects on renal oxygenation ratios in different subject populations is an important result. Further experimentation is required to examine whether or not these results hold for various subject pools. Many studies compare BOLD data from healthy and diseased subjects and use breath holding as a means to control for respiratory motion. We have demonstrated that breath holding does not affect measured signal intensity in healthy individuals, but may result in a rapid decrease in signal intensity in subjects with impaired kidney function. If further investigation verifies these results, breath holding effects will have to be considered in all of these studies.

Chapter 3

Using Diffusion Weighted MRI to Explore the Effects of Water Loading on Kidney Function

Filtration and concentration of blood to produce urine in the kidneys occurs largely by diffusion. In the proximal convoluted tubule, water is passively reabsorbed into the blood stream due to an induced osmotic gradient. In the loop of Henle and collecting ducts, the filtrate is further concentrated by a similar mechanism.

Because diffusion plays such a large role in kidney function, diffusion weighted imaging (DWI) has been investigated as a tool to evaluate kidney function. Differences between healthy and diseased kidneys have been shown to have differences in DWI. Mean ADC in tumors is significantly lower than that in healthy tissue (45). A correlation between GFR and ADC in hydronephrotic kidneys has been demonstrated (46). Namimoto *et.al* studied ADC in chronic

renal failure (CRF), acute renal failure (ARF) and renal artery stenosis (RAS) (47). There has been little work done using water loading to change DWI contrast, however, Sigmund *et.al* found that hydration state changes the measured diffusion coefficient (18).

When large amounts of water are consumed, the blood volume increases resulting in a lower osmolality of blood plasma causing more water to move to the extracellular and intracellular space. When the blood volume increases due to water consumption, reabsorption of sodium in the nephrons is restricted, resulting in a decrease in passive reabsorption of water. This effect has previously been seen on BOLD MR images as an increase in concentration of oxygenated blood (13). In this study we see if these changes are reflected in the apparent diffusion measured by DWI. Because the kidney is so highly perfused, diffusion modelling of the kidney must take this into account. Intravoxel incoherent motion (IVIM; Eq. 3.1) modelling accomplishes this [Le Bihan, 1988] by modelling the signal to have bi-exponential decay with respect to b-value. In this equation, S is the diffusion weighted signal, S_0 is the signal without diffusion weighting, f is the fraction of perfusion, D is the coefficient of true diffusion and D* is the coefficient of pseudodiffusion. In some studies, D_P is calculated (D_P = D + D*) instead of D*.

$$S = S_0((1-f)e^{-bD} + fe^{-b(D+D*)}) \tag{3.1}$$

By plotting log(S/S0) against b, D, D* and f can be calculated as the slope of point with large b-value, the slope of points with b <100, and the y-intercept of the line made by points with b <100, respectively. By using small b-values to consider perfusion, IVIM has been found to give more accurate results than apparent diffusion coefficient (ADC) calculations assuming a mono-exponential decay (40).

3.1 Hypothesis

It has already been demonstrated that an hour after rehydration, the apparent diffusion increases compared to dehydrated kidneys (18). We hypothesize that immediately after water loading there will be a temporary decrease in diffusion as the tissue is still dehydrated and less water is being reabsorbed.

3.2 Methods

Healthy subjects (ages 23-29) with no history of kidney disease and taking no medications affecting kidney function or blood pressure were se-

lected for this study. DWI was performed on six healthy individuals (3 male, 3 female) before and several times after water loading. Imaging was repeated without water loading on a separate date on four of the subjects to assess measurement repeatability. All scanning was performed using a General Electric (GE) Healthcare 3T Discovery MR750 MRI (GE Healthcare, Milwaukee, WI) and receive-only 32 channel torso phased array coil. DWI imaging parameters were as follows: slice thickness 6.0 mm; 5 b-values (0, 20, 50, 75, 500 s/mm^2); 3 diffusion directions; 1 signal average; field of view 380x380 mm^2; matrix 256x256; TR/TE 2400/66 ms. Breath holding was used to control for abdominal motion. Each diffusion direction was acquired during separate breath holds.

DWI images were acquired before water loading, immediately after (0 min), and at 7.3 min, 15 min, and 22.5 min (figure 3.1). During water loading, 20mL/kg of water was consumed over 10 minutes, and 5 minutes was allowed for getting the subject into the scanner and running localizers. For control scans, DWI images were acquired at 0, 7.5, 15, and 22.5 minutes (figure 3.1).

Image registration between b-values was performed using a linear image registration tool in FSL (56; 57; 58). ROIs were drawn on T2 weighted images using AFNI image analysis software (55). $9mm^2$ ROIs (4 voxels) were drawn in the medulla and cortex for all three directions at all time points, and to

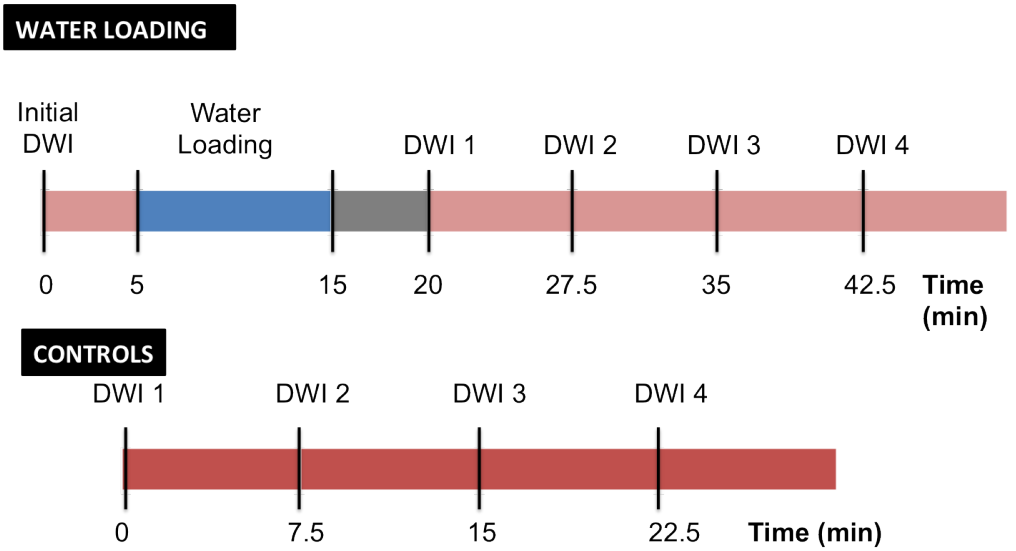

Figure 3.1: Scanning paradigm for water load (top) and control (bottom) subjects

examine the effects of having more signal averages, larger ROIs were drawn to cover the entire kidney volume (left and right) in only the anterior/posterior direction. Using in-house software written in Matlab [Mathworks, Natick, MA], diffusion and perfusion parameters were estimated in two ways. First, initial perfusion fraction (f), and pseudodiffusion (D*) were calculated as the y-intercept and slope of the line made by the data collected with b-value less than 100s/ mm^2 on a semi-log plot, and true diffusion (D) was calculated as the slope between b=0 and b=500 s/ mm^2 on a semi-log plot (59). Then, data was fit to a bi-exponential intravoxel incoherent motion (IVIM) model (Eq. 3.1) with the initial f, D* and D values input as starting values.

3.3 Results

Mean R^2 fit in the whole kidney ROI, cortex and medulla ROIs were 0.9989±0.0014, 0.9671±0.0546 and 0.9381±0.0836 respectively. Model fit was consistently better when larger ROIs were used. This is evident in the plots in figure 3.2 showing the data and model fit for baseline scans from a single subject in all three ROIs. Resultant f, D* and D values calculated both using the slope and intercept method and curve fitting method are shown in table 3.1. At baseline, mean values from water loading subjects calculated using the slope and intercept method were f=-0.2066±0.0145, D*=0.0016±0.0002 and D=0.0022±0.0002. Using the curve fitting method, mean values were f=0.0311±0.0100, D*=1.1101±0.1592 and D=0.0021±0.0002 using the whole kidney ROI. R^2 fit was consistently higher for data averaged from larger ROIs.

Figure 3.3 summarizes how well different parameters agree with expected values taken from another publication (1). It shows the values calculated for f, D* and D using both methods for each subject in the water loading study at each time point. The normal ranges of values are f: 0.234 ± 0.0934 , D: 0.0021 ± 0.0003 mm^2/s and D*: 0.1108 ± 0.0124 mm^2/s (1). For these plots, values obtained from the full kidney ROIs were used, as they were more consistent. The reported range of values were calculated using ROIs in the cortex. This shows that calculating D* using the slope of the first few points

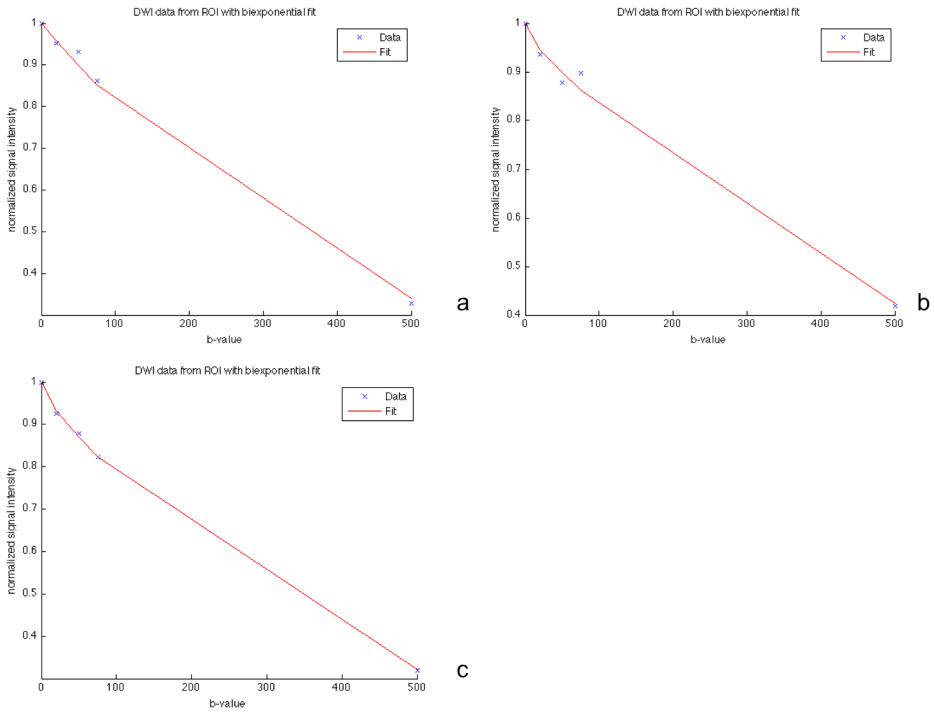

Figure 3.2: Plots show data and fit bi-exponential from (a) cortex, (b) medulla and (c) whole kidney ROIs from a single subject at baseline. R2 fits are 0.9434, 0.9776 and 0.9998 respectively.

Initial Results

Whole Kidney

	Pre-water load			0 min			7.5 min			15 min			22.5 min		
Subject	D	D*	f	D	D*	f	D	D*	f	D	D*	f	D	D*	f
1	0.0020	0.0013	-0.1856	0.0021	0.0016	-0.2295	0.0022	0.0017	-0.2309	0.0022	0.0016	-0.2394	0.0021	0.0018	-0.2408
2	0.0024	0.0017	-0.2038	0.0023	0.0019	-0.2204	0.0022	0.0024	-0.2674	0.0023	0.0030	-0.3085	0.0024	0.0026	-0.2971
3	0.0020	0.0014	-0.1959	0.0021	0.0013	-0.1763	0.0020	0.0013	-0.1569	0.0021	0.0014	-0.1822	0.0020	0.0012	-0.1724
4	0.0022	0.0018	-0.2240	0.0021	0.0015	-0.1822	0.0023	0.0017	-0.1996	0.0021	0.0016	-0.1930	0.0021	0.0018	-0.2083
5	0.0023	0.0018	-0.2198	0.0024	0.0022	-0.2402	0.0023	0.0018	-0.2121	0.0024	0.0020	-0.2122	0.0024	0.0016	-0.1917
6	0.0022	0.0016	-0.2106	0.0023	0.0005	-0.1247	0.0021	0.0014	-0.1917	0.0025	0.0007	-0.1332	0.0024	0.0014	-0.2000

Medulla

	Pre-water load			0 min			7.5 min			15 min			22.5 min		
Subject	D	D*	f	D	D*	f	D	D*	f	D	D*	f	D	D*	f
1	0.0014	0.0017	0.2202	0.0010	0.0009	0.0916	0.0011	0.0006	0.0782	0.0012	0.0010	0.1097	0.0011	0.0011	0.1191
2	0.0011	0.0006	0.0963	0.0011	0.0003	0.0214	0.0013	0.0009	0.1386	0.0011	0.0014	0.1340	0.0011	0.0012	0.1013
3	0.0009	0.0010	0.1165	0.0008	0.0007	0.1143	0.0008	0.0009	0.1050	0.0008	0.0009	0.1193	0.0011	0.0005	0.0764
4	0.0022	0.0019	0.2266	0.0014	0.0012	0.2595	0.0017	0.0014	0.3357	0.0027	0.0027	0.4449	0.0016	0.0037	0.4756
5	0.0013	0.0011	0.1199	0.0014	0.0031	0.3311	0.0014	0.0028	0.2979	0.0016	0.0035	0.2730	0.0012	0.0015	0.1086
6	0.0012	0.0010	0.0805	0.0012	0.0013	0.1289	0.0011	0.0014	0.1344	0.0012	0.0020	0.2247	0.0013	0.0027	0.2759

Cortex

	Pre-water load			0 min			7.5 min			15 min			22.5 min		
Subject	D	D*	f	D	D*	f	D	D*	f	D	D*	f	D	D*	f
1	0.0013	0.0006	0.0504	0.0013	0.0010	0.0907	0.0013	0.0009	0.1064	0.0013	0.0010	0.1141	0.0012	0.0018	0.1689
2	0.0013	0.0008	0.0720	0.0012	0.0007	0.0612	0.0013	0.0006	0.0664	0.0013	0.0015	0.1454	0.0014	0.0010	0.0869
3	0.0012	0.0019	0.1978	0.0011	0.0008	0.0755	0.0011	0.0008	0.0670	0.0012	0.0005	0.0587	0.0013	0.0024	0.2619
4	0.0025	0.0015	0.1371	0.0013	0.0021	0.2247	0.0019	0.0019	0.2035	0.0029	0.0024	0.2331	0.0013	0.0022	0.2211
5	0.0011	0.0006	0.0573	0.0016	0.0033	0.2923	0.0015	0.0025	0.1459	0.0017	0.0013	0.1590	0.0015	0.0025	0.1993
6	0.0015	0.0011	0.1393	0.0013	0.0014	0.1146	0.0012	0.0018	0.1565	0.0014	0.0015	0.1525	0.0013	0.0011	0.1149

Curve Fitting Results

Whole Kidney

	Pre-water load				0 min				7.5 min				15 min				22.5 min			
Subject	D	D*	f	R-square	D	D*	f	R-square	D	D*	f	R-square	D	D*	f	R-square	D	D*	f	R-square
1	0.0019	1.1635	0.0374	0.9989	0.0020	1.2306	0.0592	0.9996	0.0020	1.4141	0.0510	0.9998	0.0021	1.4386	0.0585	0.9997	0.0020	0.0951	0.0624	0.9989
2	0.0023	0.8809	0.0134	0.9994	0.0022	0.9306	0.0217	0.9998	0.0019	0.0123	0.1206	0.9996	0.0021	0.0225	0.0815	1.0000	0.0022	0.0688	0.0610	0.9999
3	0.0019	1.2379	0.0366	0.9996	0.0020	1.3507	0.0172	0.9985	0.0020	1.2582	0.0077	0.9992	0.0020	1.1881	0.0199	0.9995	0.0019	1.2483	0.0308	0.9987
4	0.0022	1.1988	0.0318	0.9998	0.0013	0.0025	0.5000	0.9985	0.0022	1.2646	0.0151	0.9994	0.0012	0.0030	0.5000	0.9986	0.0021	0.1307	0.0259	0.9993
5	0.0022	1.2420	0.0267	0.9998	0.0013	0.0033	0.5000	0.9993	0.0014	0.0027	0.5000	0.9991	0.0015	0.0024	0.5000	0.9985	0.0023	1.1420	0.0095	0.9993
6	0.0021	0.9374	0.0408	0.9984	0.0013	0.0031	0.5000	0.9920	0.0020	1.4610	0.0307	0.9994	0.0024	0.0005	0.1705	0.9962	0.0023	1.1549	0.0237	0.9987

Medulla

	Pre-water load				0 min				7.5 min				15 min				22.5 min			
Subject	D	D*	f	R-square	D	D*	f	R-square	D	D*	f	R-square	D	D*	f	R-square	D	D*	f	R-square
1	0.0011	4.9952	0.1040	0.9571	0.0009	3.5631	0.0197	0.9482	0.0011	0.7907	0.0170	0.9789	0.0011	0.4795	0.0196	0.9929	0.0011	0.0423	0.0213	0.9956
2	0.0010	0.4585	0.0226	0.9564	0.0009	0.0000	0.0001	0.9385	0.0012	1.0375	0.0527	0.9887	0.0008	0.0027	0.1667	0.9459	0.0009	0.0006	0.1667	0.9597
3	0.0008	0.0081	0.0263	0.9122	0.0006	0.0000	0.0000	0.6503	0.0007	0.0000	0.0002	0.7889	0.0006	0.0000	0.0000	0.7008	0.0010	3.4615	0.0035	0.9593
4	0.0013	2.7655	0.1152	0.9690	0.0011	2.5296	0.1369	0.9901	0.0013	3.6339	0.1654	0.9974	0.0022	3.5716	0.1810	0.9962	0.0010	0.6930	0.2298	0.9929
5	0.0012	0.3505	0.0083	0.9776	0.0010	0.1225	0.1802	0.8210	0.0010	0.4555	0.1955	0.9921	0.0012	3.5170	0.0020	0.7459	0.0010	0.0000	0.0000	0.8465
6	0.0008	0.0041	0.2357	0.9516	0.0011	3.5000	0.0291	0.9943	0.0009	0.0096	0.1675	0.9924	0.0011	0.0776	0.0686	0.9994	0.0012	0.6881	0.0638	0.9870

Cortex

	Pre-water load				0 min				7.5 min				15 min				22.5 min			
Subject	D	D*	f	R-square	D	D*	f	R-square	D	D*	f	R-square	D	D*	f	R-square	D	D*	f	R-square
1	0.0012	4.9590	0.0176	0.9827	0.0012	0.0004	0.0037	0.9757	0.0011	0.3369	0.1667	0.9951	0.0012	0.3264	0.0132	0.9946	0.0010	0.0469	0.1667	0.9976
2	0.0013	0.0000	0.0261	0.9848	0.0011	3.4958	0.0004	0.9799	0.0011	4.8883	0.1695	0.9854	0.0011	0.5760	0.1677	0.9906	0.0013	0.0000	0.0033	0.9778
3	0.0011	0.5436	0.0318	0.9476	0.0010	1.0791	0.0037	0.9863	0.0010	0.0000	0.0063	0.9893	0.0011	0.3875	0.0117	0.9908	0.0110	0.0438	0.0666	0.9947
4	0.0014	0.3326	0.0150	0.9630	0.0011	0.0181	0.1023	0.9925	0.0017	0.0166	0.0459	0.9977	0.0023	0.0085	0.0218	0.9902	0.0010	0.3249	0.1688	0.9905
5	0.0011	0.0000	0.0011	0.9434	0.0010	0.0054	0.2887	0.9794	0.0013	0.0123	0.1799	0.9967	0.0015	0.0294	0.0759	0.9894	0.0014	0.0050	0.0377	0.9670
6	0.0011	0.0048	0.2357	0.9651	0.0011	0.0012	0.1669	0.9652	0.0010	3.5276	0.1668	0.9886	0.0010	0.0024	0.2357	0.9956	0.0009	3.5218	0.2361	0.9878

Table 3.1: Summary of diffusion and perfusion parameters during water loading experiment.

is much more accurate than the curve fitting method, with many of the curve fitting results being orders of magnitude larger than expected. Many D values fell within the expected range, but there seems to be more success with the slope calculation approach. For calculation of f, curve fitting was closer, but still less than the expected values. Because f calculated as the y-intercept on a semi-log plot was consistently negative and f calculated using curve fitting had such large variance, no further analysis of f was performed.

Change in diffusion and pseudodiffusion over time in water loading and control subjects are shown in the cortex, medulla and whole kidney (figure 3.4). These figures used values obtained from the initial slope calculations, as these were more consistent. A repeated measures 2-way ANOVA found no significant difference in D or D* between water load and control groups or over time.

Because the temporal response to water loading varied between individuals, the time course of D and D* measurements from each subject were plotted on the same set of axes in figure 3.5. The values used are those calculated using the slope method. No trends exist that are consistent between subjects during this time period.

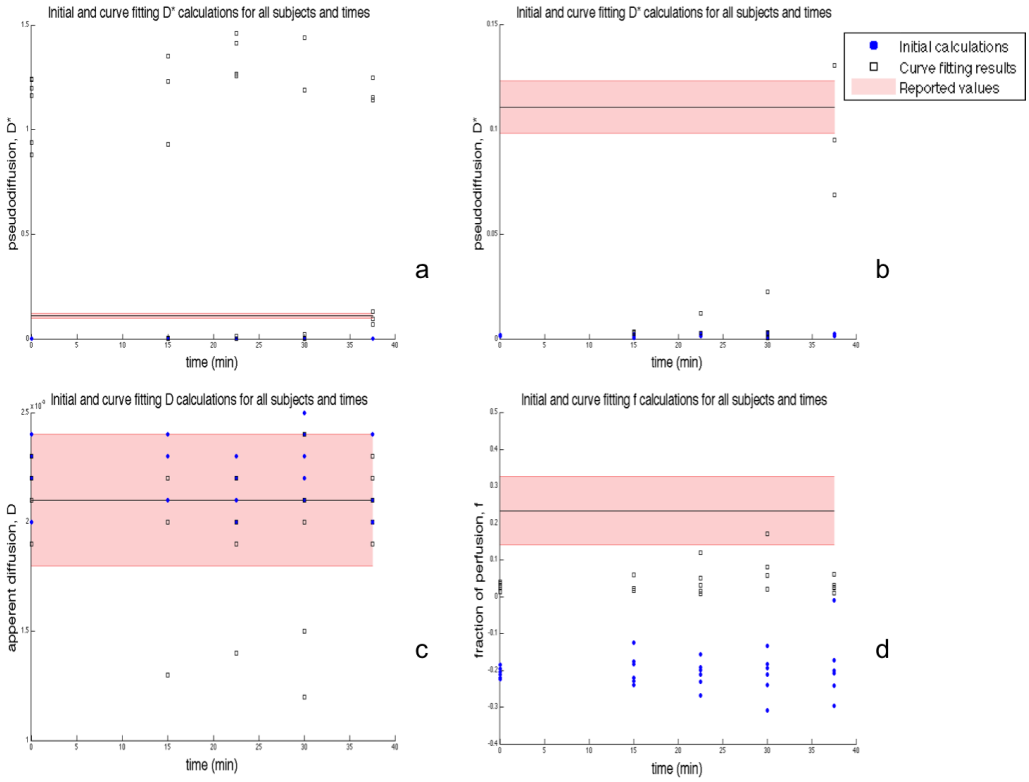

Figure 3.3: Plots showing calculated parameters using both the slope and intercept method (blue circles) and curve fitting method (squares) for (a) D*, (b) D* zoomed in to scale of expected value, (c) D, and (d) f. Overlain on the plots in red are the expected range of values according to one published study: f: 0.234 ± 0.0934 , D: 0.0021 ± 0.0003 mm^2/s and D*: 0.1108 ± 0.0124 mm^2/s (1).

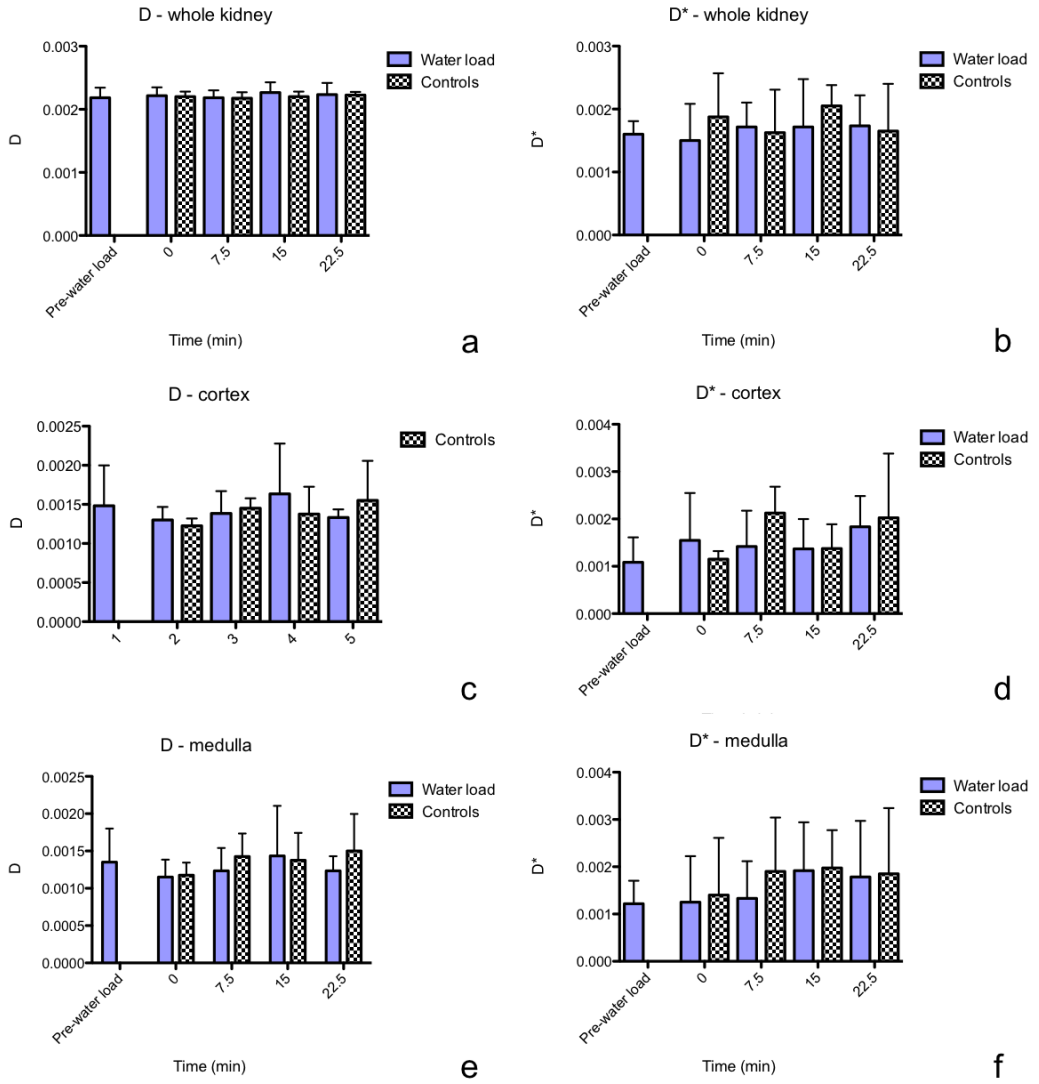

Figure 3.4: Graphs showing mean and standard deviation of D and D* in all subjects and controls for each time point in the (a-b) whole kidney, (c-d) cortex and (e-f) medulla.

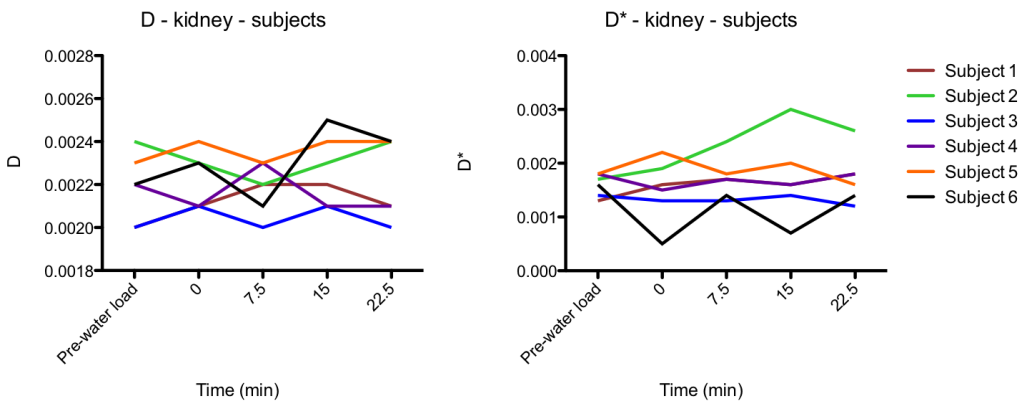

Figure 3.5: D and D* for each water load subject at all time points; calculated using slope of semi-log plot.

3.4 Discussion

The data obtained in this study fit well to a bi-exponential diffusion model. There were better fits in the data averaged from larger ROIs, reinforcing the notion that more signal averages improves accuracy of the results as shown by Zhang *et.al* (43). The values calculated using the slope of a semi-log plot were more consistent, and in the case of D*, closer to the expected range. Fraction of perfusion calculated as the y-intercept of the line made by values obtained at smaller b-values were at the anticipated order of magnitude in the cortex and medulla ROIs, but consistently negative in the whole-kidney ROIs. The values obtained from curve fitting were constrained to be greater that zero and less than 0.5, and the resultant values ranged from $5x10^{-8}$ to 0.5, so were deemed unreliable. The values for D were closer to the expected

range when calculated by slope, but the constraint that D should be smaller when calculated using curve fitting was used since some of the calculated ADC should be the result of perfusion. Since only one b-value greater than 100 is used, the error in this measurement will have a large impact on the calculated diffusion coefficient. The accuracy and precision of the calculated values could likely be improved by increasing both the number of excitations (NEX) in signal acquisition and by acquiring more b-values. With the imaging approach being used in this study, breath holding was used to avoid respiratory motion and so scan duration was an issue. Use of respiratory triggering would allow for more excitations.

The values obtained from curve fitting varied greatly from the values reported by previous studies (41; 18; 60; 1). The curve fitting results from this study and various published studies are summarized in table 3.2. Here, D is comparable to other studies, but D* and f are quite different. The standard deviation reported by these other papers are not much better than the ones found here, suggesting that their curve fitting approach gave a similar variability as seen here.

To test the effects of the initial conditions used in curve fitting, calculations were repeated on baseline scans of water load subjects using the average values reported by Ichikawa *et.al* (1) as initial conditions for the

	Results	Zhang *et. al*, 2010 ** (41)	Sigmund *et. al*, 2012*,** (18)	Rheinheimer *et. al*, 2012 (60)	Ichikawa *et. al*, 2012 (1)
B0	3T	3T	3T	1.5T	1.5T
No. of b-values	5	16	8	9	12
No. of subjects	6	3	10	30	80
Subject age	22-29	20-39	22-32	36-80	60.5 ± 13.5
Signal averages	1	9		4	3
ROI	Whole kidney	Whole kidney	Whole cortex	Whole cortex	Cortex (5 voxels)
D (mean ± SD) mm^2/s	0.0021 ± 0.0002	0.0017 ± 0.0002	0.0020 ± 0.00006	0.0019 ± 0.0001	0.0021 ± 0.0003
D* (mean ± SD) mm^2/s	1.1101 ± 0.1592	0.0001 ± 0.0034	0.0004 ± 0.0061	Not reported	0.1108 ± 0.0124
f (mean ± SD)	0.0311 ± 0.0100	0.32 ± 0.08	0.1869 ± 0.0256	0.1832 ± 0.0252	0.234 ± 0.0934

Table 3.2: Summary of diffusion and perfusion parameters reported in literature. (* SD from this study are for intra-subject variability; ** In these studies, original calculations found D_P and D* was calculated from this for the purpose of this comparison.)

curve fitting. The new means and standard deviations were D=0.0018±0.0004, D*=0.1118±0.2417, and f=0.2042±0.2298. The R^2 fit stayed the same in four of the six cases, and in the other two cases R^2 fit decreased. This shows that the results are highly dependant on initial conditions used in curve fitting. Using reported values forced the calculated parameters to be closer to those found previously, but a large degree of variability still exists. At present, there is no consensus in the literature on what these values should be, so a data driven approach is likely the better option.

No changes in diffusion or perfusion coefficients were seen as a result of water loading. Images were acquired 15 - 45 minutes after the initiation of the water loading period. Subtle changes may be made apparent if the scanning protocol can be optimized to give more reliable results. It has already been demonstrated that an increase in the apparent diffusion coefficient is observed approximately 1 hour after the initiation of water loading (18), but we have shown that these effects are not observed at earlier time points. Changes in diffusion during and immediately after the initiation of rehydration have not yet been studied. Future studies may consider examining this time period to see if the kidneys initial response to water loading can be measured.

Chapter 4

Fractal Analysis of Renal BOLD MRI Before and After Water Loading

Fractal patterns appear to be random, but are in fact complex deterministic patterns. They are characterized as having self-similarity at multiple scales: as the pattern is magnified, the sub-structures take on the same form as the larger features (Fig. 4.1). Common examples from everyday life include the branching patterns of trees or the contour of mountain ranges. Temporal signals can also have fractal characteristics. In these cases, the variability of the signal is similar to the variability seen when the finer fluctuations of a smaller time period are examined. Measurements are not exactly the same at different scales, but rather are statistically similar. Measurements taken at high temporal resolution are proportional to the same measurements taken over the entire time course measured at a lower temporal resolution. For the purpose of this study, fractal properties of the frequency characteristics of a time signal were evaluated to determine if the signal is fractal as proposed by

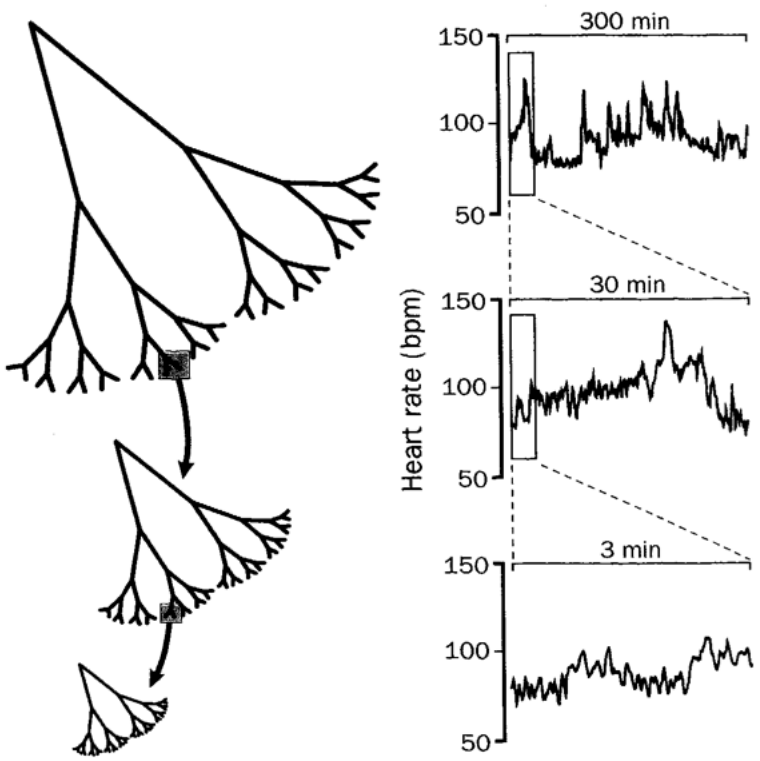

Figure 4.1: Example of fractal geometry (left), with self-similarity at multiple *spatial* scales. Similarly, temporal fluctuations in heart rate (right) show statistical self-similarity at different *temporal* scales (2).

Eke *et.al* (61). Signals were considered fractal if they exhibited the following relationship:

$$|A(f)|^2 \propto cf^{-\beta} \tag{4.1}$$

for at least a 2 decade range. Here, A is the amplitude of the fast Fourier transform (FFT) at frequency f, c is a constant and β is the exponent.

This relationship is called a power law relationship. If the logarithm of the FFT is plotted against the logarithm of the frequency space, -β is the slope of the line. Fractal dimension (FD) or Hurst coefficient (H = 2-FD for a 1 dimensional signal) are the measures used to describe the fractal nature of a signal. FD ranges from 1 to 2, and H, therefore, ranges from 0 to 1. A lower H (higher FD) indicates that a signal is more rough or anti-correlated and a higher H (lower FD) indicates that a signal is more smooth or correlated. White noise (no correlation) has H = 0.5 (FD = 1.5).

Fractal signals can be classified as fractional Gaussian noise (fGn) or fractional Brownian motion (fBm). fGn are stationary signals and fBm are non-stationary signals with stationary increments. fBm signals can be converted to fGn by taking successive differences between elements of the series, and conversely, fGn signals can be converted to fBm by calculating the cumulative sum.

Fractal analysis on real-time BOLD data has been used to study microvascular organization in diseases such as rectal carcinoma (62) and Alzheimers disease (63). Wardlaw *et.al* contributed the lower FD in a tumor as compared to healthy tissue to high microvascular vasoactivity (62). Warsi *et.al* found that low FD correlated with markers of Alzheimers disease, signifying a less complex signal (63).

The effects of water loading with an ion replacement drink have been investigated in a previous study (54). That study was looking for changes in the contribution of the cardiac peak in the BOLD signal post water loading. Results were inconclusive. In this study, real-time BOLD data from healthy kidneys were analyzed to determine whether signal variations are fractal, and if so whether they can be characterized as fGn or fBm. Should the signal be shown to be fractal, analysis will be done to determine whether fractal characteristics are modified shortly after water loading.

4.1 Hypothesis

It has been shown that water loading increases oxygenation in young, healthy subjects due to a decrease in active reabsorption in the ascending thick limb of the loop of Henle (19). We hypothesize that, should the BOLD signal from the kidney be fractal, the reduction in activity after water loading will result in an increase in the Hurst coefficient and, therefore, a decrease in the fractal dimension.

4.2 Methods

The protocol outlined in this study was approved by our research ethics board (REB) as per the declaration of Helsinki. 7 healthy subjects with no history of kidney disease were scanned (mean age 24±3 years).

All scans were done using a General Electric (GE) Healthcare 3T HD Signa MRI (GE Healthcare, Milwaukee, WI) and receive-only 8 channel torso phased array coil (USA Instruments In., Aurora, OH, USA). Respiratory data was collected concurrently with BOLD scanning using the MRI scanner respiratory bellows. Following a 3-plane localizer, sagittal multi-phase FIESTA images were acquired to prescribe an oblique coronal offset used for BOLD scanning (Fig. 4.2). This was previously determined to reduce in-plane motion during BOLD imaging (54). BOLD scanning was performed before and after water loading using a T2* weighted (BOLD) GRE EPI sequence (TR/TE=250/35ms, flip=70^o, FOV=30cm 96x96 matrix, 3 slices 5mm thick, 0mm skip, oblique-coronal plane, 2400 temporal points, 10 minutes total time). During the pre-water load scan, subjects were instructed to breathe quietly. Following the initial BOLD scan, subjects came off the scanner table and drank 1L/30kg body mass of a 50% v/v G2 $Gatorade^{TM}$ (The Gatorade Company, Chicago, IL; 30 calories, 115mg Na+, 30mg K+, and 7g carbohydrates per

Figure 4.2: Plane selection used in data acquisition. Imaging plane is chosen along the long axis of the kidney: the direction of motion during breathing.

200mL) solution over 15 minutes. The subjects were then put back in the MRI and the BOLD imaging sequence was repeated.

Images were processed with a template-matching algorithm (Fig. 4.3) originally developed to track coronary motion (64) and previously used for kidney analysis (54), followed by a linear image registration tool in FSL (56; 57; 58) for further motion correction. Regions of interest (ROI) were selected in renal medulla and renal cortex using AFNI (55), and time course BOLD data was exported to MATLAB (Mathworks, Natick, MA) for analysis using an in-house developed algorithm based on work done by Eke et al. (61). In this algorithm, Fourier analysis is done to determine if the signals frequency spectrum follows a power law relationship. If it does, β is calculated as the

slope of the log-log plot. If $\beta < 1$, the signal is fGn, and if $\beta > 1$, the signal is fBm. In this algorithm, signals with $0.38 < \beta < 1.04$ are considered too close to the border to be classified. Analysis of fGn voxels was repeated using the dispersion method, which is more accurate for analyzing fGn signals, and fBm voxels were analyzed using the scaled windowed variance method.

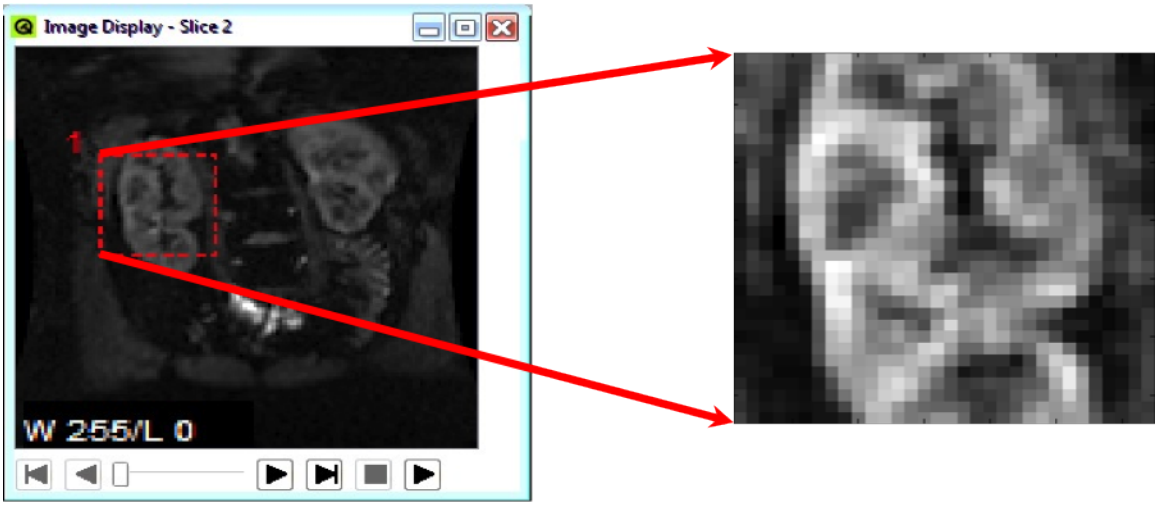

Figure 4.3: Example template selection in first BOLD image (left) and subsequent extracted template in all subsequent time points (right).

Dispersion analysis is based on standard deviation at varying window lengths (τ). Specifically, (H-1) is the slope of log[SD(τ)/SD(τ_0)] versus log (τ/ τ_0), where τ_0 is a reference window.

$$logSD(\tau) = (H-1)log(\frac{\tau}{\tau_0}) + logSD(\tau_0). \tag{4.2}$$

In scaled windowed variance analysis, the Hurst coefficient is calculated using the average standard deviation of the signal in non-overlapping windows measured at varying window length, τ. This relationship is shown in Eq. 4.3.

$$logSD(\tau) = HlogSD(\frac{\tau}{\tau_0}) + logSD(\tau_0). \tag{4.3}$$

The Hurst coefficient relates to β and FD by equations 4.4 and 4.5.

$$H = \frac{\beta + 1}{2} \tag{4.4}$$

$$FD = 2 - H \tag{4.5}$$

4.3 Results

Representative plots of the initial frequency analysis from the cortex and medulla are shown in figure 4.4. The peak at -0.5 in the medulla is from

reparatory fluctuations. A linear trend exists over a 2-decade range, so fractal analysis was deemed logical to continue. For comparison, figure 4.5 shows the same initial frequency analysis done on a voxel containing only noise. The signal is far less linear over the first two decades. FD maps were calculated using the temporal methods suggested by Eke *et.al* (61). A representative FD map using this analysis method and corresponding map of R^2 fits pre- and post-water loading are shown in figure 4.6. There is very little, if any, contrast between the kidney and surrounding tissue seen in the FD map. This was consistent across all subjects. R^2 values are high throughout the majority of the image. It should be noted that large R^2 fits are expected as a result of smoothing the time points (61). Upon visual inspection, it appears as though FD increased in the kidney after water loading, particularly in the lower portion of the cortex.

ROIs were drawn in the cortex and medulla of BOLD data acquired before and after water loading. Because there was still some residual kidney motion of some subjects, even after motion correction, voxels that remained in either the cortex or medulla for the duration of the scan were chosen, and voxels near edges where motion was a problem were rejected. The average number of voxels in cortex and medulla ROIs were 51$\pm$12 and 29$\pm$10 respectively. Mean FD calculations using the dispersion and scaled windowed vari-

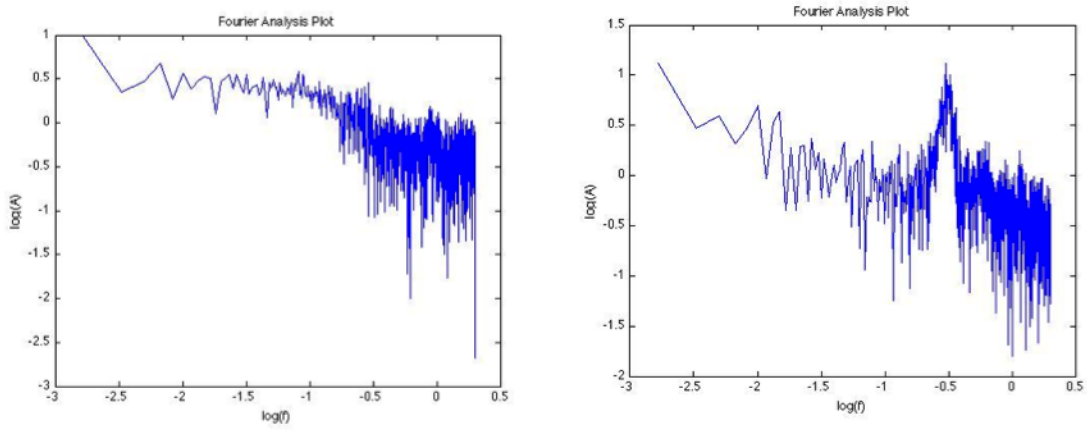

Figure 4.4: Representative plots of log (A) versus log (f), where A is amplitude of the FFT and f is the frequency, from a single voxel from the cortex (left) and medulla (right) from one subject.

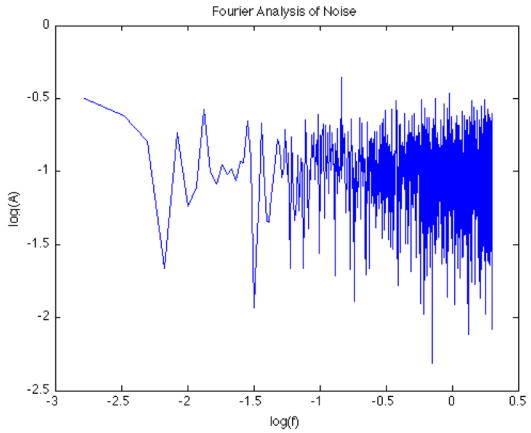

Figure 4.5: log(A) versus log(f), where A is amplitude of the FFT taken from a voxel containing only noise and f is the frequency.

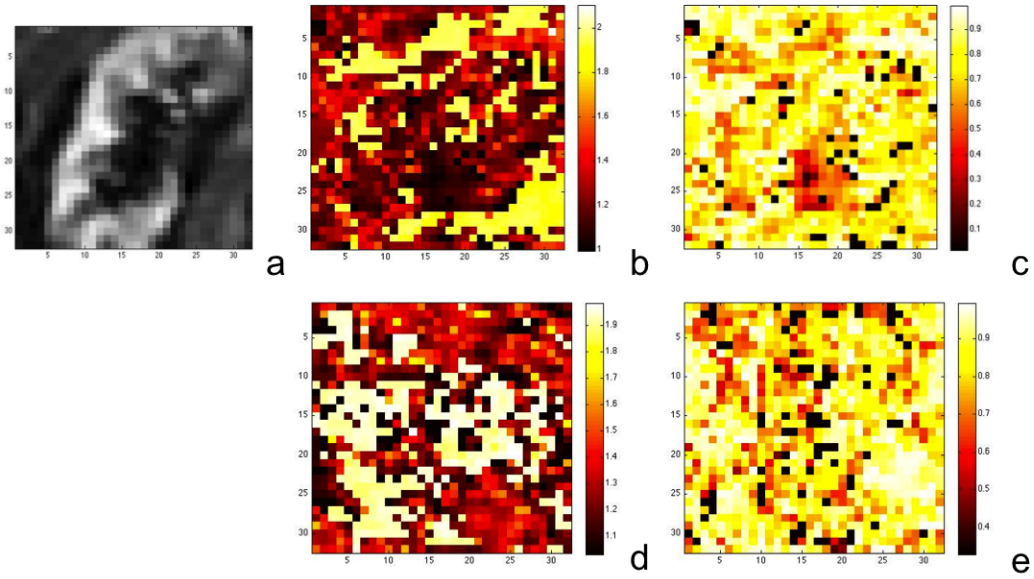

Figure 4.6: Single time point of BOLD scan after motion correction from one subject (a) with corresponding FD map (b) and R^2 fit map (c). Also shown are the FD map (d) and corresponding R^2 fit map from the same subject post water loading.

ance analysis methods in the cortex and medulla are summarized in table 4.1. Voxels in the medulla and cortex ranged from 0% to 100% fGn, with averages of 33.2±33.1% and 32.6±24.9% respectively. At baseline, mean FD in the cortex was 1.59±0.28 and mean FD in the medulla was 1.64±0.33. After water loading, mean FD in the cortex and medulla were 1.65±0.24 and 1.73±0.28 respectively. A repeated measures ANOVA found no significant difference before and after water loading ($p = 0.4063$) or between cortex and medulla ($p = 0.6288$). These results are summarized in figure 4.7.

	Subject	Pre-water loading Median FD ± SD	Post-water loading Median FD ± SD	% change in FD
Cortex	1	1.90 ± 0.09	1.73 ± 0.04	-8.95
	2	1.55 ± 0.33	1.88 ± 0.22	+21.29
	3	1.21 ± 0.22	1.36 ± 0.34	+12.40
	4	1.31 ± 0.35	1.40 ± 0.36	+6.87
	5	1.48 ± 0.28	1.44 ± 0.24	-2.70
	6	1.84 ± 0.06	1.84 ± 0.27	0.00
	7	1.86 ± 0.25	1.87 ± 0.20	+0.54
Medulla	1	1.90 ± 0.35	1.76 ± 0.03	-7.37
	2	1.38 ± 0.31	1.90 ± 0.23	+37.68
	3	1.28 ± 0.32	1.25 ± 0.17	-2.34
	4	1.20 ± 0.32	1.93 ± 0.27	+60.83
	5	1.92 ± 0.24	1.41 ± 0.16	-26.56
	6	1.92 ± 0.04	1.92 ± 0.26	0.00
	7	1.86 ± 0.33	1.90 ± 0.16	+2.15

Table 4.1: Fractal dimension (FD) pre- and post-water loading.

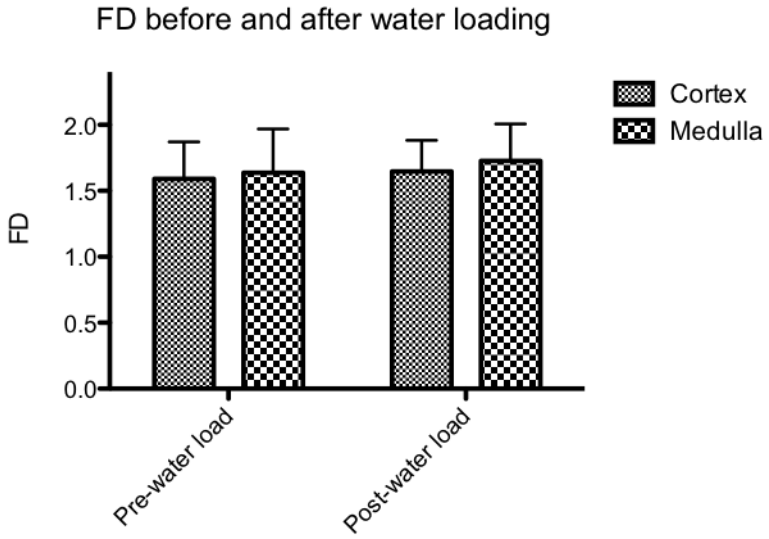

Figure 4.7: Mean ± SD FD in cortex and medulla from all subjects before and after water loading. No significant differences were observed between cortex and medulla or pre- and post-water loading.

4.4 Discussion

Based on the linear trend seen in Fourier analysis, the renal BOLD signal has been evaluated as fractal. All voxels examined from all subjects showed this linear trend for at least a two-decade range. This is the data range suggested by Eke *et.al* (61). It should be noted that, in many subjects, this trend does not continue past the two-decade range. This does not have an affect on the fit of the fractal model as fractal analysis only considers the low frequencies: in this study, only the lowest 1/8 of the total frequency spectrum was used. This method of analysis produced high variability across voxels and poor contrast between the kidney and surrounding tissue. There was also no

statistically significant change in fractal dimension in the cortex or medulla as a result of water loading. As a result, fractal analysis provides no insight into the effects of water loading on the renal BOLD signal.

The large variability in conjunction with good fitting to the model was an unexpected result. This high variability may be attributed to artifacts in the data. Respiratory motion should not be an issue because the respiratory frequency is not in the frequency range used for analysis. There may still be motion artifacts from peristalsis of the intestines. Partial volume effects may also be a concern, as the data acquired for this study had voxel size is 3x3x5 mm, which is poor in comparison to the size of the kidney. Contribution of different renal tissues such as medulla and cortex in each voxel may change as the kidney is moved and compressed during breathing. Even with these problems, it is promising that the signal tends to fit a fractal model. It is possible that improved motion correction and resolution may result in less variability in FD measurements.

Chapter 5

Conclusion

5.1 Summary of results

Breath holding results show no effect on BOLD signal intensity in young, healthy subjects. This result confirms that using breath holding as a means of reducing respiratory motion will not affect the study results for this subject pool. A significant change in BOLD signal intensity was observed in a single subject with impaired renal function. Further investigation is required to determine how breath holding affects BOLD signal intensity for subjects of varying age and disease state.

The renal BOLD signal was found to have fractal characteristics. Specifically, the frequency spectrum showed a power law relationship. No changes were measured using this technique between pre- and post-water loading scans during the time period examined. Because the signal appears to behave fractally, this technique may be a good candidate for functional kidney studies with different objectives. It is also possible that fractal dimension may change

after a longer time period. It may be worthwhile to consider fractal analysis after one hour, or using urine output to determine when hydration has been effective.

DWI also remained unchanged as a result of water loading during the post-water loading time period examined. Both of the methods used to calculate diffusion and perfusion parameters had disadvantages. The slope/intercept calculations done on a semi-log plot gave more consistent results, but the fraction of perfusion was often found to be negative, which is not logical. With the curve fitting approach, constraints can be placed to force the parameters to be more reasonable. Since, in the case of the fraction of perfusion, the calculated values frequently reached these enforced limits, the results are not thought to accurately represent the physiology. Improvements to the DWI protocol should be made to address these issues. If respiratory gating is used to prevent respiratory motion artefacts instead of breath holding, longer scan times can be used, which would allow for more signal averages and more b-values.

5.2 Consideration of Respiratory Motion

In both the breath holding and fractal analysis studies, data obtained during free breathing were used. Although the motion correction techniques used greatly improved registration between time points or b-values as shown

in figure 5.1, it was not perfect and only accounted for in-plane motion. The effects of registering the data may also be introducing changes that propagate to the final measurements. The use of these motion correction tools assumes that the signal from anywhere in a particular tissue type is similar enough that through plane motion will not affect the final results. A three-dimensional deformable registration algorithm should be developed to improve future free breathing studies.

5.3 Improvement of DWI Protocol

To attempt to get diffusion and perfusion parameters that are closer to those reported in other studies, a single subject was scanned using a larger number of b-values and signal averages. 38 b-values were used from 0 to 800, and two signal averages were acquired at each b. For this scan, respiratory gating was used to reduce respiratory artefacts. The resultant data plotted with a bi-exponential fit is shown in figure 5.2. The data fits the curve very well, with an R^2 fit of 0.9983. The parameters calculated from this fit were D = 0.0022, D* = 0.0237 and f = 13.57%. The diffusion coefficient agrees well with reported values, as did the values calculated using fewer b-values. Pseudodiffusion and fraction of perfusion calculated from this data agree with

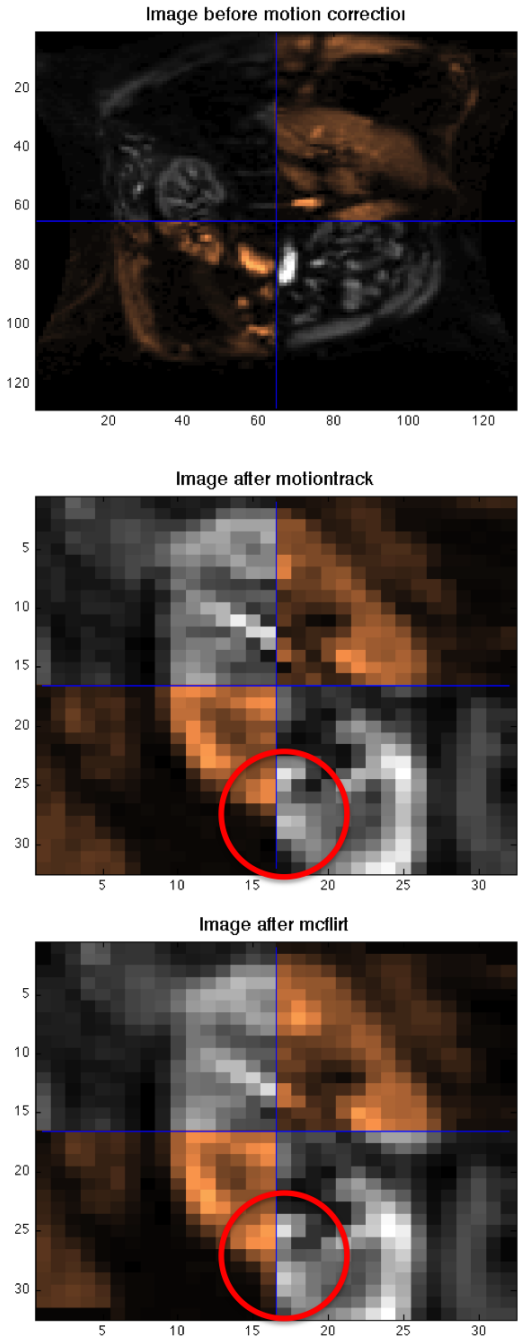

Figure 5.1: Figures show two time points of a BOLD scan before any motion correction (top), after motiontrack template matching (middle) and after mcflirt image registration in FSL (bottom). Quadrants in grayscale are from one time point and quadrants in copper are from the other time point. The red circles on the bottom two images highlights an area of improved registration between the two steps.

the reported values better than results from fewer b-values. Although these results are taken from only one subject, these results are encouraging.

The bi-exponential fit accounts for the tissue water and blood water being two separate pools. In the kidneys, there is a third pool: filtrate in the nephrons. These filtrate protons move at a different speed than the other two water pools. For this reason, it may be interesting to see if this third component can be seen in the diffusion data. As a preliminary experiment, the same data as used in the above calculations is fit with a tri-exponential curve (figure 5.3). R^2 fit is 0.9867. Not enough work has been done to say whether or not the third component is visible, but in this single case, the curve does not seem to follow the data as well.

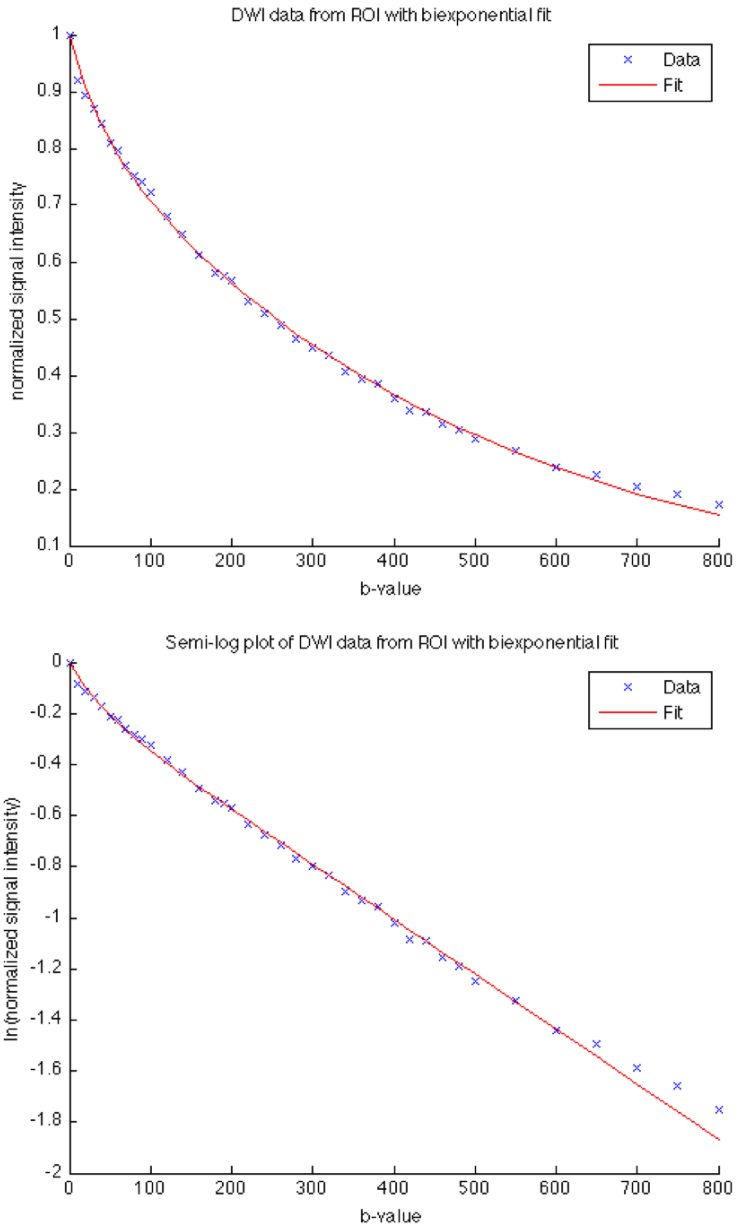

Figure 5.2: Data and bi-exponential fit with many b-values (top) and the same results on a semi-log plot (bottom). R^2 fit = 0.9983.

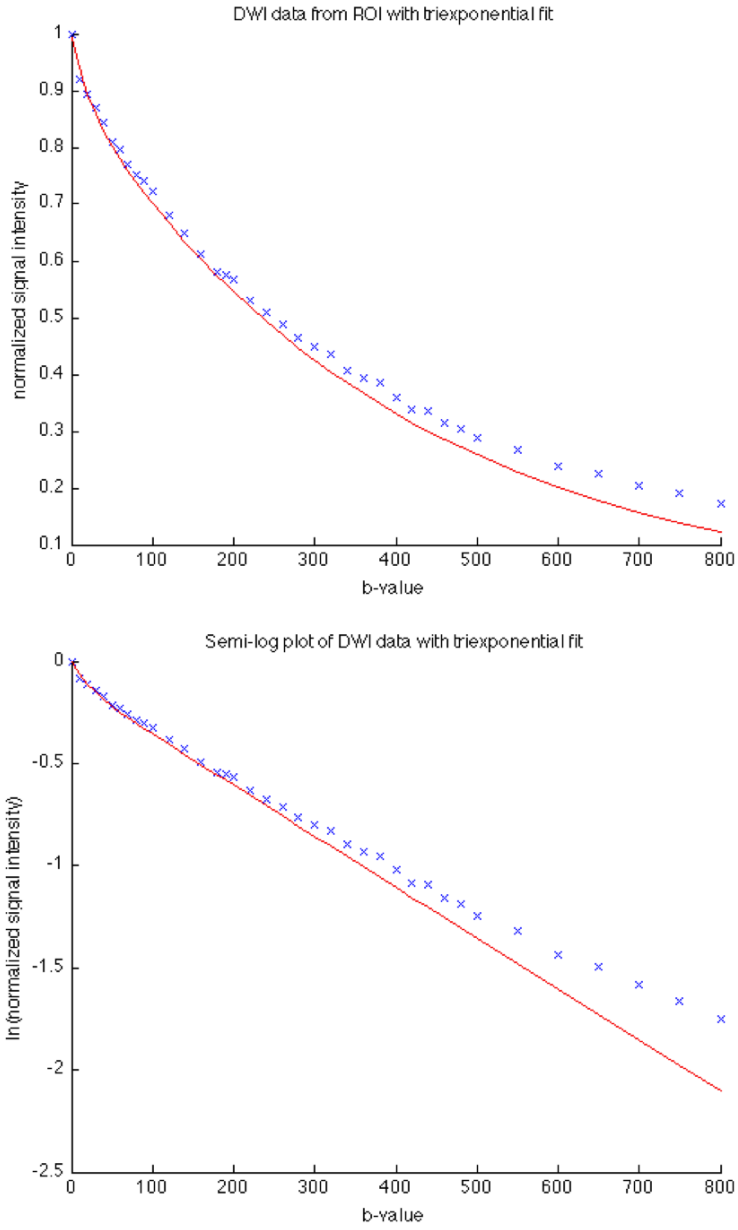

Figure 5.3: Plot showing data acquired at many b-values, with a tri-exponential curve fit to it (top) and the same results on a semi-log plot (bottom). Fitting is worse compared to the bi-exponential model. R^2 fit =0.9867.

Bibliography

[1] S. Ichikawa, U. Motosugi, T. Ichikawa, K. Sano, H. Morisaka, and T. Araki, "Intravoxel incoherent motion imaging of the kidney: alterations in diffusion and perfusion in patients with renal dysfunction," *Magnetic resonance imaging*, vol. 31, pp. 414–417, Apr 2013. CI: Copyright (c) 2013; JID: 8214883; 2012/03/17 [received]; 2012/07/11 [revised]; 2012/08/30 [accepted]; 2012/10/25 [aheadofprint]; ppublish.

[2] A. L. Goldberger, "Non-linear dynamics for clinicians: chaos theory, fractals, and complexity at the bedside," *Lancet*, vol. 347, pp. 1312–1314, May 11 1996. LR: 20081121; JID: 2985213R; OTO: NASA; ppublish.

[3] M. Chonchol and D. M. Spiegel, *The Patient With Chronic Kidney Disease*, p. 185. Manual of Nephrology, Philadelphia, PA, USA: Lippincott Williams & Wilkins, 7 ed., 2009.

[4] N. Hackstein, H. Kooijman, S. Tomaselli, and W. S. Rau, "Glomerular filtration rate measured using the patlak plot technique and contrast-enhanced dynamic mri with different amounts of gadolinium-dtpa," *Journal of magnetic resonance imaging : JMRI*, vol. 22, pp. 406–414, Sep 2005. LR: 20061115; CI: (c) 2005; JID: 9105850; 0 (Contrast Media); 66108-95-0 (Iohexol); 73334-07-3 (iopromide); 7440-54-2 (Gadolinium); ppublish.

[5] N. Hackstein, J. Heckrodt, and W. S. Rau, "Measurement of single-kidney glomerular filtration rate using a contrast-enhanced dynamic gradient-echo sequence and the rutland-patlak plot technique," *Journal of magnetic resonance imaging : JMRI*, vol. 18, pp. 714–725, Dec 2003. LR: 20041117; CI: Copyright 2003; JID: 9105850; 0 (Contrast Media); 80529-93-7 (Gadolinium DTPA); ppublish.

[6] D. Laurent, K. Poirier, J. Wasvary, and M. Rudin, "Effect of essential hypertension on kidney function as measured in rat by dynamic mri," *Magnetic resonance in medicine : official journal of the Society of Magnetic Resonance in Medicine / Society of Magnetic Resonance in Medicine*, vol. 47, pp. 127–134, Jan 2002. LR: 20031114; CI: Copyright 2002; JID: 8505245; 0 (Calcium Channel Blockers); 0 (Contrast Media); 52-53-9 (Verapamil); 80529-93-7 (Gadolinium DTPA); ppublish.

[7] V. S. Lee, H. Rusinek, M. E. Noz, P. Lee, M. Raghavan, and E. L. Kramer, "Dynamic three-dimensional mr renography for the mea-

surement of single kidney function: initial experience," *Radiology*, vol. 227, pp. 289–294, Apr 2003. LR: 20071114; GR: K23-DK02814/DK/NIDDK NIH HHS/United States; JID: 0401260; 0 (Radiopharmaceuticals); 65454-61-7 (Technetium Tc 99m Pentetate); 2003/02/28 [aheadofprint]; ppublish.

[8] I. Mendichovszky, M. Pedersen, J. Frokiaer, T. Dissing, N. Grenier, P. Anderson, K. McHugh, Q. Yang, and I. Gordon, "How accurate is dynamic contrast-enhanced mri in the assessment of renal glomerular filtration rate? a critical appraisal," *Journal of magnetic resonance imaging : JMRI*, vol. 27, pp. 925–931, Apr 2008. CI: (c) 2008; JID: 9105850; 0 (Contrast Media); 80529-93-7 (Gadolinium DTPA); RF: 20; ppublish.

[9] T. Chopra, K. Kandukurti, S. Shah, R. Ahmed, and M. Panesar, "Understanding nephrogenic systemic fibrosis," *International journal of nephrology*, vol. 2012, p. 912189, 2012. LR: 20130219; JID: 101546753; OID: NLM: PMC3501952; 2012/06/21 [received]; 2012/08/22 [revised]; 2012/08/28 [accepted]; 2012/11/04 [epublish]; ppublish.

[10] J. J. Cohen and D. E. Kamm, *Renal metabolism: relation to renal function*, p. 147. The Kidney, Philadelphia: Saunders, 1981.

[11] M. W. Taal, G. M. Chertow, P. A. Marsden, K. Skorecki, A. S. L. Yu, and B. M. Brenner, *Brenner & Rector's The Kidney*, vol. 1. Philadelphia, PA: Elsevier Saunders, 9 ed., 2012.

[12] M. E. Chamberlin and L. J. Mandel, "Na+-k+-atpase activity in medullary thick ascending limb during short-term anoxia," *The American Journal of Physiology*, vol. 252, pp. F838–43, May 1987. LR: 20071115; GR: AM-26816/AM/NIADDK NIH HHS/United States; JID: 0370511; 0 (Adenine Nucleotides); 7440-09-7 (Potassium); EC 3.6.3.9 (Sodium-Potassium-Exchanging ATPase); ppublish.

[13] P. V. Prasad, R. R. Edelman, and F. H. Epstein, "Noninvasive evaluation of intrarenal oxygenation with bold mri," *Circulation*, vol. 94, pp. 3271–3275, Dec 15 1996. LR: 20071114; GR: R0-18078/PHS HHS/United States; JID: 0147763; 0 (Diuretics); 0 (Oxyhemoglobins); 54-31-9 (Furosemide); 59-66-5 (Acetazolamide); 7782-44-7 (Oxygen); CIN: Circulation. 1996 Dec 15;94(12):3067-8. PMID: 8989108; ppublish.

[14] M. Burg, L. Stoner, J. Cardinal, and N. Green, "Furosemide effect on isolated perfused tubules," *American Journal of Physiology–Legacy Content*, vol. 225, no. 1, pp. 119–124, 1973.

[15] M. Brezis, Y. Agmon, and F. H. Epstein, "Determinants of intrarenal oxygenation. i. effects of diuretics," *American Journal of Physiology-Renal Physiology*, vol. 267, no. 6, pp. F1059–F1062, 1994.

[16] H. Rennke and B. Denker, *Renal Pathophysiology: the Essentials*. Baltamore, USA: Lippincott Williams & Wilkins, 2 ed., 2007.

[17] S. M. Tumkur, A. T. Vu, L. P. Li, L. Pierchala, and P. V. Prasad, "Evaluation of intra-renal oxygenation during water diuresis: a time-resolved study using bold mri," *Kidney international*, vol. 70, pp. 139–143, Jul 2006. LR: 20110926; GR: DK-53221/DK/NIDDK NIH HHS/United States; GR: R01 DK053221-09/DK/NIDDK NIH HHS/United States; JID: 0323470; 0 (Cyclooxygenase Inhibitors); 22204-53-1 (Naproxen); 7732-18-5 (Water); 7782-44-7 (Oxygen); CIN: Kidney Int. 2006 Jul;70(1):10-1. PMID: 16810286; NIHMS157863; OID: NLM: NIHMS157863; OID: NLM: PMC2919062; 2006/03/29 [aheadofprint]; ppublish.

[18] E. E. Sigmund, P.-H. Vivier, D. Sui, N. A. Lamparello, K. Tantillo, A. Mikheev, H. Rusinek, J. S. Babb, P. Storey, and V. S. Lee, "Intravoxel incoherent motion and diffusion-tensor imaging in renal tissue under hydration and furosemide flow challenges," *Radiology*, vol. 263, no. 3, pp. 758–769, 2012.

[19] P. V. Prasad and F. H. Epstein, "Changes in renal medullary po2 during water diuresis as evaluated by blood oxygenation level-dependent magnetic resonance imaging: effects of aging and cyclooxygenase inhibition," *Kidney international*, vol. 55, pp. 294–298, Jan 1999. LR: 20110926; GR: DK 18078/DK/NIDDK NIH HHS/United States; GR: DK 53221/DK/NIDDK NIH HHS/United States; GR: M01-RRO-1032/RR/NCRR NIH HHS/United States; GR: R01 DK053221-02/DK/NIDDK NIH HHS/United States; GR: R01 DK053221-04/DK/NIDDK NIH HHS/United States; JID: 0323470; 0 (Cyclooxygenase Inhibitors); 15687-27-1 (Ibuprofen); 363-24-6 (Dinoprostone); 7782-44-7 (Oxygen); NIHMS223440; OID: NLM: NIHMS223440; OID: NLM: PMC2918873; ppublish.

[20] F. H. Epstein, A. Veves, and P. V. Prasad, "Effect of diabetes on renal medullary oxygenation during water diuresis," *Diabetes care*, vol. 25, no. 3, pp. 575–578, 2002.

[21] M. F. Muller, P. V. Prasad, D. Bimmler, A. Kaiser, and R. R. Edelman, "Functional imaging of the kidney by means of measurement of the

apparent diffusion coefficient," *Radiology*, vol. 193, pp. 711–715, Dec 1994. LR: 20041117; JID: 0401260; ppublish.

[22] G. M. Danovitch, *Handbook of kidney transplantation*. Lippincott Williams & Wilkins, 2009.

[23] A. S. Levey, J. P. Bosch, J. B. Lewis, and T. Greene, "A more accurate method to estimate glomerular filtration rate from serum creatinine: a new prediction equation," 1999.

[24] D. W. Cockcroft and M. H. Gault, "Prediction of creatinine clearance from serum creatinine," *Nephron*, vol. 16, no. 1, pp. 31–41, 1976.

[25] A. S. Levey, L. A. Stevens, C. H. Schmid, Y. Zhang, A. F. Castro, H. I. Feldman, J. W. Kusek, P. Eggers, F. V. Lente, and T. Greene, "A new equation to estimate glomerular filtration rate," *Annals of Internal Medicine*, vol. 150, no. 9, p. 604, 2009.

[26] D. Goldsmith, S. Jayawardene, and P. Ackland, *ABC of Kidney Disease*. Massachusettes, USA: Blackwell Publishing Ltd., 2007.

[27] J. C. Jennette, J. L. Olson, M. M. Schwartz, and F. G. Silvia, *Heptinstalls Pathology of the Kidney*, vol. 2. Philadelphia, PA: Lippincott Williams & Wilkins, 6 ed., 2007.

[28] M. Brezis and S. Rosen, "Hypoxia of the renal medulla–its implications for disease," *The New England journal of medicine*, vol. 332, pp. 647–655, Mar 9 1995. LR: 20061115; JID: 0255562; 7782-44-7 (Oxygen); RF: 70; ppublish.

[29] P. V. Prasad, Q. Chen, J. W. Goldfarb, F. H. Epstein, and R. R. Edelman, "Breath-hold r2* mapping with a multiple gradient-recalled echo sequence: application to the evaluation of intrarenal oxygenation," *Journal of magnetic resonance imaging : JMRI*, vol. 7, pp. 1163–1165, Nov-Dec 1997. LR: 20061115; JID: 9105850; ppublish.

[30] M. Pedersen, J. Morkenborg, T. Dissing, and J. Frokiaer, "Quantitative blood oxygenation in the kidney," in *International Society for Magnetic Resonance in Medicine*, 2001.

[31] S. C. Simon-Zoula, L. Hofmann, A. Giger, B. Vogt, P. Vock, F. J. Frey, and C. Boesch, "Non-invasive monitoring of renal oxygenation using bold-mri: a reproducibility study," *NMR in biomedicine*, vol. 19, pp. 84–89, Feb 2006. CI: 2006; JID: 8915233; 7782-44-7 (Oxygen); ppublish.

[32] D. Niles, S. Fain, N. Artz, Y. Huang, K. Vigen, A. Djamali, and E. . Sadowski, "Longitudinal evaluation of renal oxygenation in kidney donors and recipients using bold mri," in *International Society For Magnetic Resonance in Medicine Annual Meeting*, 2011.

[33] F. H. Epstein and P. Prasad, "Effects of furosemide on medullary oxygenation in younger and older subjects," *Kidney international*, vol. 57, pp. 2080–2083, May 2000. LR: 20071114; GR: MO1-RR1032/RR/NCRR NIH HHS/United States; JID: 0323470; 15687-27-1 (Ibuprofen); 54-31-9 (Furosemide); 7782-44-7 (Oxygen); ppublish.

[34] L. P. Li, S. Halter, and P. V. Prasad, "Blood oxygen level-dependent mr imaging of the kidneys," *Magnetic resonance imaging clinics of North America*, vol. 16, pp. 613–25, viii, Nov 2008. LR: 20110926; GR: DK-53221/DK/NIDDK NIH HHS/United States; GR: R01 DK053221-11/DK/NIDDK NIH HHS/United States; JID: 9422762; 7782-44-7 (Oxygen); RF: 106; NIHMS76536; OID: NLM: NIHMS76536; OID: NLM: PMC2652565; ppublish.

[35] H. J. Michaely, L. Metzger, S. Haneder, J. Hansmann, S. O. Schoenberg, and U. I. Attenberger, "Renal bold-mri does not reflect renal function in chronic kidney disease," *Kidney international*, vol. 81, pp. 684–689, Apr 2012. LR: 20121127; JID: 0323470; 60-27-5 (Creatinine); 7782-44-7 (Oxygen); CIN: Kidney Int. 2012 Apr;81(7):613-4. PMID: 22419042; CIN: Kidney Int. 2012 Oct;82(8):934; author reply 935. PMID: 23018827; CIN: Kidney Int. 2012 Oct;82(8):934-5; author reply 935. PMID: 23018828; 2012/01/11 [aheadofprint]; ppublish.

[36] M. Nangaku, "Chronic hypoxia and tubulointerstitial injury: a final common pathway to end-stage renal failure," *Journal of the American Society of Nephrology : JASN*, vol. 17, pp. 17–25, Jan 2006. LR: 20061115; JID: 9013836; 0 (Hypoxia-Inducible Factor 1); EC 1.14.11.2 (Procollagen-Proline Dioxygenase); RF: 76; 2005/11/16 [aheadofprint]; ppublish.

[37] T. Inoue, E. Kozawa, H. Okada, K. Inukai, S. Watanabe, T. Kikuta, Y. Watanabe, T. Takenaka, S. Katayama, J. Tanaka, and H. Suzuki, "Noninvasive evaluation of kidney hypoxia and fibrosis using magnetic resonance imaging," *Journal of the American Society of Nephrology : JASN*, vol. 22, pp. 1429–1434, Aug 2011. LR: 20120925; JID: 9013836; 7782-44-7 (Oxygen); OID: NLM: PMC3148697; 2011/07/14 [aheadofprint]; ppublish.

[38] W. J. Yin, F. Liu, X. M. Li, L. Yang, S. Zhao, Z. X. Huang, Y. Q. Huang, and R. B. Liu, "Noninvasive evaluation of renal oxygenation in diabetic nephropathy by bold-mri," *European Journal of Radiology*, vol. 81, pp. 1426–1431, Jul 2012. CI: Copyright (c) 2011; JID: 8106411; 7782-44-7 (Oxygen); 2011/01/25 [received]; 2011/03/06 [revised]; 2011/03/11 [accepted]; 2011/04/05 [aheadofprint]; ppublish.

[39] J. Neugarten, "Renal bold-mri and assessment for renal hypoxia," *Kidney international*, vol. 81, pp. 613–614, Apr 2012. JID: 0323470; 11096-26-7 (Erythropoietin); 7782-44-7 (Oxygen); CON: Kidney Int. 2012 Apr;81(7):684-9. PMID: 22237750; CON: Kidney Int. 2002 Feb;61(2):542-6. PMID: 11849394; ppublish.

[40] H.-J. Wittsack, R. S. Lanzman, M. Quentin, J. Kuhlemann, J. Klasen, G. Pentang, C. Riegger, G. Antoch, and D. Blondin, "Temporally resolved electrocardiogram-triggered diffusion-weighted imaging of the human kidney: Correlation between intravoxel incoherent motion parameters and renal blood flow at different time points of the cardiac cycle," *Investigative radiology*, vol. 47, no. 4, p. 226, 2012.

[41] J. L. Zhang, E. E. Sigmund, H. Chandarana, H. Rusinek, Q. Chen, P. H. Vivier, B. Taouli, and V. S. Lee, "Variability of renal apparent diffusion coefficients: limitations of the monoexponential model for diffusion quantification," *Radiology*, vol. 254, pp. 783–792, Mar 2010. LR: 20110725; JID: 0401260; OID: NLM: PMC2851010; 2010/01/20 [aheadofprint]; ppublish.

[42] D. LeBihan, E. Breton, D. Lallemand, M. L. Aubin, J. Vignaud, and M. Laval-Jeantet, "Separation of diffusion and perfusion in intravoxel incoherent motion mr imaging," *Radiology*, vol. 168, pp. 497–505, Aug 1988. LR: 20061115; JID: 0401260; ppublish.

[43] J. L. Zhang, E. E. Sigmund, H. Rusinek, H. Chandarana, P. Storey, Q. Chen, and V. S. Lee, "Optimization of b-value sampling for diffusion-weighted imaging of the kidney," *Magnetic resonance in medicine : official journal of the Society of Magnetic Resonance in Medicine / Society of Magnetic Resonance in Medicine*, vol. 67, pp. 89–97, Jan 2012. CI: Copyright (c) 2011; JID: 8505245; 2011/02/21 [received]; 2011/04/05 [accepted]; 2011/06/23 [aheadofprint]; ppublish.

[44] D. LeBihan and R. Turner, "The capillary network: a link between ivim and classical perfusion," *Magnetic resonance in medicine : official journal of the Society of Magnetic Resonance in Medicine / Society of*

Magnetic Resonance in Medicine, vol. 27, pp. 171–178, Sep 1992. LR: 20051116; JID: 8505245; RF: 44; ppublish.

[45] E. Squillaci, G. Manenti, M. Cova, M. D. Roma, R. Miano, G. Palmieri, and G. Simonetti, "Correlation of diffusion-weighted mr imaging with cellularity of renal tumours," *Anticancer Research*, vol. 24, pp. 4175–4179, Nov-Dec 2004. JID: 8102988; ppublish.

[46] S. Toyoshima, K. Noguchi, H. Seto, M. Shimizu, and N. Watanabe, "Functional evaluation of hydronephrosis by diffusion-weighted mr imaging. relationship between apparent diffusion coefficient and split glomerular filtration rate," *Acta Radiologica (Stockholm, Sweden : 1987)*, vol. 41, pp. 642–646, Nov 2000. LR: 20041117; JID: 8706123; 0 (Radiopharmaceuticals); 65454-61-7 (Technetium Tc 99m Pentetate); ppublish.

[47] T. Namimoto, Y. Yamashita, K. Mitsuzaki, Y. Nakayama, Y. Tang, and M. Takahashi, "Measurement of the apparent diffusion coefficient in diffuse renal disease by diffusion-weighted echo-planar mr imaging," *Journal of magnetic resonance imaging : JMRI*, vol. 9, pp. 832–837, Jun 1999. LR: 20041117; JID: 9105850; ppublish.

[48] P. Heusch, H. J. Wittsack, P. Kropil, D. Blondin, M. Quentin, J. Klasen, G. Pentang, G. Antoch, and R. S. Lanzman, "Impact of blood flow on diffusion coefficients of the human kidney: A time-resolved ecg-triggered diffusion-tensor imaging (dti) study at 3t," *Journal of magnetic resonance imaging : JMRI*, Jul 13 2012. CI: Copyright (c) 2012; JID: 9105850; aheadofprint.

[49] M. E. Thomason, B. E. Burrows, J. D. Gabrieli, and G. H. Glover, "Breath holding reveals differences in fmri bold signal in children and adults," *NeuroImage*, vol. 25, pp. 824–837, Apr 15 2005. LR: 20071114; GR: MH-61426/MH/NIMH NIH HHS/United States; GR: RR-09784/RR/NCRR NIH HHS/United States; JID: 9215515; 7782-44-7 (Oxygen); 2004/05/21 [received]; 2004/11/19 [revised]; 2004/12/09 [accepted]; ppublish.

[50] K. K. Kwong, I. Wanke, K. M. Donahue, T. L. Davis, and B. R. Rosen, "Epi imaging of global increase of brain mr signal with breath-hold preceded by breathing o2," *Magnetic resonance in medicine : official journal of the Society of Magnetic Resonance in Medicine / Society of Magnetic Resonance in Medicine*, vol. 33, pp. 448–452, Mar 1995. LR: 20061115; JID: 8505245; 0 (Hemoglobins); 124-38-9 (Carbon Dioxide); 7782-44-7 (Oxygen); 9008-02-0 (deoxyhemoglobin); ppublish.

[51] M. K. Stehling, F. Schmitt, and R. Ladebeck, "Echo-planar mr imaging of human brain oxygenation changes," *Journal of magnetic resonance imaging : JMRI*, vol. 3, pp. 471–474, May-Jun 1993. LR: 20041117; JID: 9105850; 0 (Hemoglobins); 7782-44-7 (Oxygen); 9008-02-0 (deoxyhemoglobin); ppublish.

[52] A. E. Stillman, X. Hu, and M. Jerosch-Herold, "Functional mri of brain during breath holding at 4 t," *Magnetic resonance imaging*, vol. 13, no. 6, pp. 893–897, 1995. LR: 20071115; GR: P41RR08079/RR/NCRR NIH HHS/United States; JID: 8214883; 7782-44-7 (Oxygen); ppublish.

[53] T. Q. Li, A. Kastrup, A. M. Takahashi, and M. E. Moseley, "Functional mri of human brain during breath holding by bold and fair techniques," *NeuroImage*, vol. 9, pp. 243–249, Feb 1999. LR: 20071115; CI: Copyright 1999; GR: NCRR P-41 09784/RR/NCRR NIH HHS/United States; JID: 9215515; ppublish.

[54] B. Boyd and M. D. Noseworthy, *Assessment of kidney funtion using bold magnetic resonance imaging during induced diuresis*. Hamilton, Ontario, Canada: McMaster University, 2010.

[55] R. W. Cox, "Afni: software for analysis and visualization of functional magnetic resonance neuroimages," *Computers and biomedical research, an international journal*, vol. 29, pp. 162–173, Jun 1996. LR: 20071114; GR: MH51358/MH/NIMH NIH HHS/United States; JID: 0100331; ppublish.

[56] M. Jenkinson, C. F. Beckmann, T. E. Behrens, M. W. Woolrich, and S. M. Smith, "Fsl," *NeuroImage*, vol. 62, no. 2, pp. 782–790, 2012.

[57] M. W. Woolrich, S. Jbabdi, B. Patenaude, M. Chappell, S. Makni, T. Behrens, C. Beckmann, M. Jenkinson, and S. M. Smith, "Bayesian analysis of neuroimaging data in fsl," *NeuroImage*, vol. 45, no. 1 Suppl, pp. S173–S186, 2009.

[58] S. M. Smith, M. Jenkinson, M. W. Woolrich, C. F. Beckmann, T. Behrens, H. Johansen-Berg, P. R. Bannister, M. D. Luca, I. Drobnjak, and D. E. Flitney, "Advances in functional and structural mr image analysis and implementation as fsl.," *NeuroImage*, vol. 23, p. S208, 2004.

[59] D. LeBihan and R. Turner, "Intravoxel incoherent motion (ivim) imaging using spin-echos," in *The Society of Magnetic Resonance In Medicine*, p. 67, 1990.

[60] S. Rheinheimer, F. Schneider, B. Stieltjes, C. Morath, M. Zeier, H. U. Kauczor, and P. Hallscheidt, "Ivim-dwi of transplanted kidneys: re-

duced diffusion and perfusion dependent on cold ischemia time," *European Journal of Radiology*, vol. 81, pp. e951–6, Sep 2012. CI: Copyright (c) 2012; JID: 8106411; 2012/04/30 [received]; 2012/06/15 [revised]; 2012/06/17 [accepted]; 2012/07/10 [aheadofprint]; ppublish.

[61] A. Eke, P. Herman, J. Bassingthwaighte, G. Raymond, D. Percival, M. Cannon, I. Balla, and C. Ikrnyi, "Physiological time series: distinguishing fractal noises from motions," *European Journal of Physiology*, vol. 439, no. 4, pp. 403–415, 2000.

[62] G. Wardlaw, R. Wong, and M. D. Noseworthy, "Identification of intratumour low frequency microvascular components via bold signal fractal dimension mapping," *Physica medica : PM : an international journal devoted to the applications of physics to medicine and biology : official journal of the Italian Association of Biomedical Physics (AIFB)*, vol. 24, pp. 87–91, Jun 2008. JID: 9302888; 7782-44-7 (Oxygen); 2007/11/01 [received]; 2008/01/04 [accepted]; 2008/02/21 [aheadofprint]; ppublish.

[63] M. A. Warsi, W. Molloy, and M. D. Noseworthy, "Correlating brain blood oxygenation level dependent (bold) fractal dimension mapping with magnetic resonance spectroscopy (mrs) in alzheimers disease," *Magnetic Resonance Materials in Physics, Biology and Medicine*, pp. 1–10, 2012.

[64] M. S. Sussman and G. A. Wright, "Factors affecting the correlation coefficient template matching algorithm with application to real-time 2-d coronary artery mr imaging," *Medical Imaging, IEEE Transactions on*, vol. 22, no. 2, pp. 206–216, 2003.